Chapter 4

LONGITUDINAL VEHICLE DYNAMICS

The control of longitudinal vehicle motion has been pursued at many different levels by researchers and automotive manufacturers. Common systems involving longitudinal control available on today's passenger cars include cruise control, anti-lock brake systems and traction control systems. Other advanced longitudinal control systems that have been the topic of intense research include radar-based collision avoidance systems, adaptive cruise control systems, individual wheel torque control with active differentials and longitudinal control systems for the operation of vehicles in platoons on automated highway systems.

This chapter presents dynamic models for the longitudinal motion of the vehicle. The two major elements of the longitudinal vehicle model are the vehicle dynamics and the powertrain dynamics. The vehicle dynamics are influenced by longitudinal tire forces, aerodynamic drag forces, rolling resistance forces and gravitational forces. Models for these forces are discussed in section 4.1. The longitudinal powertrain system of the vehicle consists of the internal combustion engine, the torque converter, the transmission and the wheels. Models for these components are discussed in section 4.2.

4.1 LONGITUDINAL VEHICLE DYNAMICS

Consider a vehicle moving on an inclined road as shown in Figure 4-1. The external longitudinal forces acting on the vehicle include aerodynamic drag forces, gravitational forces, longitudinal tire forces and rolling resistance forces. These forces are described in detail in the sub-sections that follow.

R. Rajamani, *Vehicle Dynamics and Control*, Mechanical Engineering Series,
DOI 10.1007/978-1-4614-1433-9_4, © Rajesh Rajamani 2012

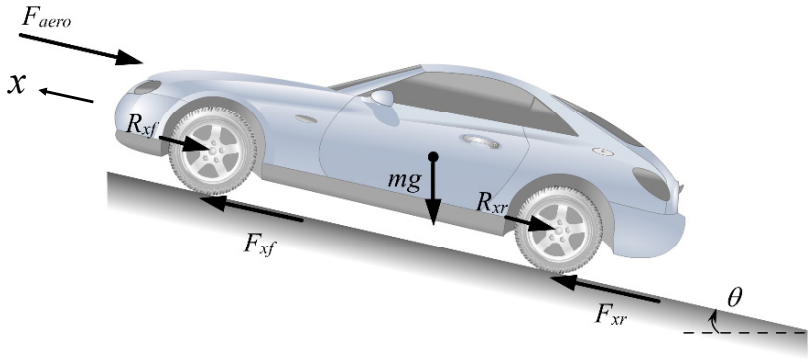

Figure 4-1. Longitudinal forces acting on a vehicle moving on an inclined road

A force balance along the vehicle longitudinal axis yields

$$m\ddot{x} = F_{xf} + F_{xr} - F_{aero} - R_{xf} - R_{xr} - mg\sin(\theta) \tag{4.1}$$

where

F_{xf} is the longitudinal tire force at the front tires

F_{xr} is the longitudinal tire force at the rear tires

F_{aero} is the equivalent longitudinal aerodynamic drag force

R_{xf} is the force due to rolling resistance at the front tires

R_{xr} is the force due to rolling resistance at the rear tires

m is the mass of the vehicle

g is the acceleration due to gravity

θ is the angle of inclination of the road on which the vehicle is traveling

The angle θ is defined to be positive clockwise when the longitudinal direction of motion x is towards the left (as in Figure 4-1). It is defined to be positive counter clockwise when the longitudinal direction of motion x is towards the right.

4.1.1 Aerodynamic drag force

The equivalent aerodynamic drag force on a vehicle can be represented as

$$F_{aero} = \frac{1}{2}\rho C_d A_F (V_x + V_{wind})^2 \tag{4.2}$$

where ρ is the mass density of air, C_d is the aerodynamic drag coefficient, A_F is the frontal area of the vehicle, which is the projected area of the vehicle in the direction of travel, $V_x = \dot{x}$ is the longitudinal vehicle velocity, V_{wind} is the wind velocity (positive for a headwind and negative for a tailwind).

Atmospheric conditions affect air density ρ and hence can significantly affect aerodynamic drag. The commonly used standard set of conditions to which all aerodynamic test data are referred to are a temperature of 15 ^oC and a barometric pressure of 101.32 kPa (Wong, 2001). The corresponding mass density of air ρ may be taken as 1.225 kg/m^3.

The frontal area A_F is in the range of 79-84 % of the area calculated from the vehicle width and height for passenger cars (Wang, 2001). According to Wang, 2001, the following relationship between vehicle mass and frontal area can be used for passenger cars with mass in the range of 800-2000 kg:

$$A_f = 1.6 + 0.00056(m - 765) \tag{4.3}$$

The aerodynamic drag coefficient C_d can be roughly determined from a coast-down test (White and Korst, 1972). In a coast down test, the throttle angle is kept at zero and the vehicle is allowed to slow under the effects of aerodynamic drag and rolling resistance. Since there is neither braking nor throttle angle inputs, the longitudinal tire force under these conditions is small and can be assumed to be zero. The road is assumed to be level with $\theta = 0$ and the wind velocity V_{wind} is assumed to be zero.

Under these conditions, the longitudinal dynamics equation can be re-written as

$$-m\frac{dV_x}{dt} = \frac{1}{2}\rho V_x^{\,2} A_F C_d + R_x \tag{4.4}$$

or

$$-\frac{dV_x}{\frac{\rho A_F C_d V_x^{\,2}}{2m}+\frac{R_x}{m}}=dt \tag{4.5}$$

Integrating equation (4.5), assuming an initial longitudinal velocity of V_0, one obtains (White and Korst, 1972)

$$t=\left[\frac{2m^2}{\rho A_F C_d R_x}\right]^{1/2}\left\{\tan^{-1}\left[V_o\left(\frac{\rho A_F C_d}{2R_x}\right)^{1/2}\right]-\tan^{-1}\left[V_x\left(\frac{\rho A_F C_d}{2R_x}\right)^{1/2}\right]\right\} \tag{4.6}$$

Let the total time for the vehicle to coast-down to a stop be $t=T$. Then, non-dimensionalizing using the parameter

$$\beta=V_o\left(\frac{\rho A_F C_d}{2R_x}\right)^{1/2} \tag{4.7}$$

yields

$$\frac{V_x}{V_o}=\frac{1}{\beta}\tan\left[\left(1-\frac{t}{T}\right)\tan^{-1}(\beta)\right] \tag{4.8}$$

In equation (4.8), V_x and t can be measured and the initial velocity V_0 is known. Equation (4.8) represents a one-parameter family, in β, of curves in which non-dimensional velocity $\frac{V_x}{V_o}$ can be plotted against non-dimensional time $\frac{t}{T}$. From such a plot, the value of β for a particular vehicle can be obtained.

Once β has been obtained from equation (4.8), then the following algebraic expressions can be used to calculate the rolling resistance and drag coefficient (White and Korst, 1972):

$$C_d = \frac{2m\beta \tan^{-1}(\beta)}{V_o T \rho A_F} \tag{4.9}$$

$$R_x = \frac{V_o m \tan^{-1}(\beta)}{\beta T} \tag{4.10}$$

These algebraic expressions are obtained by substitution of the final and initial values of time and velocity in equation (4.6) (White and Korst, 1972).

4.1.2 Longitudinal tire force

The longitudinal tire forces F_{xf} and F_{xr} are friction forces from the ground that act on the tires.

Experimental results have established that the longitudinal tire force generated by each tire depends on

a) the slip ratio (defined below),
b) the normal load on the tire and
c) the friction coefficient of the tire-road interface.

The vertical force on a tire is called the tire normal load. The normal load on a tire

a) comes from a portion of the weight of the vehicle
b) is influenced by fore-aft location of the c.g., vehicle longitudinal acceleration, aerodynamic drag forces and grade of the road.
Section 4.1.5 describes calculation of the tire normal loads.

Slip Ratio

The difference between the actual longitudinal velocity at the axle of the wheel V_x and the equivalent rotational velocity $r_{eff}\omega_w$ of the tire is called longitudinal slip. In other words, longitudinal slip is equal to $r_{eff}\omega_w - V_x$. *Longitudinal slip ratio* is defined as

$$\sigma_x = \frac{r_{eff}\omega_w - V_x}{V_x} \text{ during braking} \tag{4.11}$$

$$\sigma_x = \frac{r_{eff}\omega_w - V_x}{r_{eff}\omega_w} \text{ during acceleration} \tag{4.12}$$

An explanation of why longitudinal tire force depends on the slip ratio is provided in section 4.1.3. A more complete understanding of the influence of all three variables – slip ratio, normal force and tire-road friction coefficient – on tire force can be obtained by reading Chapter 13 of this book.

If the friction coefficient of the tire-road interface is assumed to be 1 and the normal force is assumed to be a constant, the typical variation of longitudinal tire force as a function of the slip ratio is shown in Figure 4-2.

As can be seen from the figure, in the case where longitudinal slip ratio is small (typically less than 0.1 on dry surface), as it is during normal driving, the longitudinal tire force is found to be proportional to the slip ratio. The tire force in this small-slip region can then be modeled as

$$F_{xf} = C_{\sigma f}\sigma_{xf} \tag{4.13}$$

$$F_{xr} = C_{\sigma r}\sigma_{xr} \tag{4.14}$$

where $C_{\sigma f}$ and $C_{\sigma r}$ are called the longitudinal tire stiffness parameters of the front and rear tires respectively.

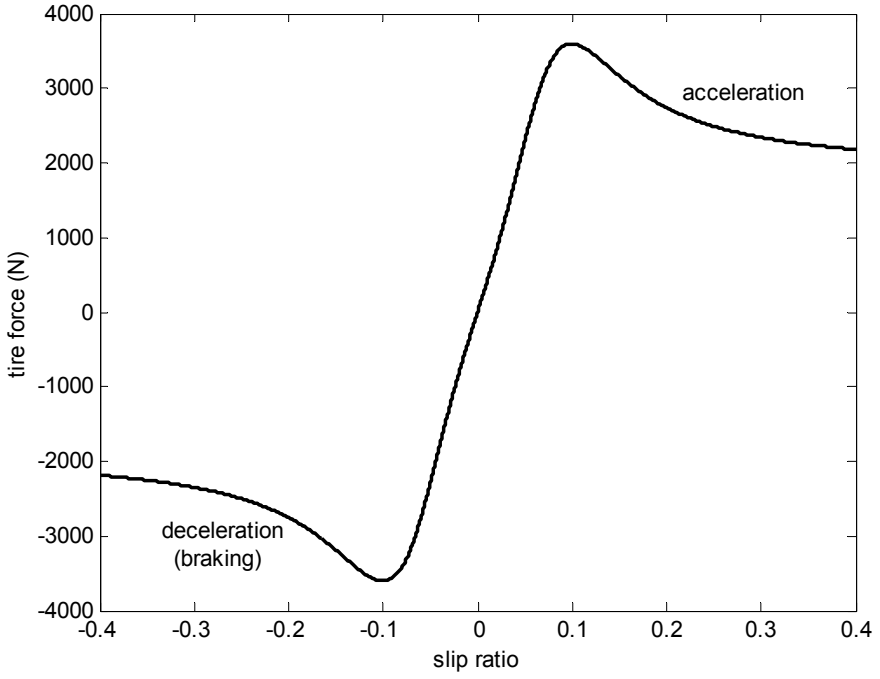

Figure 4-2. Longitudinal tire force as a function of slip ratio

If the longitudinal slip ratio is not small or if the road is slippery, then a nonlinear tire model needs to be used to calculate the longitudinal tire force. The Pacejka "Magic Formula" model or the Dugoff tire model can be used to model tire forces in this case (Pacejka and Bakker, 1993, Pacejka, 1996 and Dugoff, et. al., 1969). These models are discussed in detail in Chapter 13 of this book.

4.1.3 Why does longitudinal tire force depend on slip ?

A rough explanation of why the longitudinal tire force depends on slip ratio can be seen from Figure 4-3.

The lower portion of Figure 4-3 shows a schematic representation of deformation of the tread elements of the tire. The tread elements are modeled as a series of independent springs that undergo longitudinal deformation and resist with a constant longitudinal stiffness. Such a model of the tire is called a "brush" model or an "elastic foundation" model (Pacejka, 1991, Dixon, 1991).

Let the longitudinal velocity of the wheel be V_x and its rotational velocity be ω_w. Then the net velocity at the treads, as shown in Figure 4-3 is $r_{eff}\omega_w - V_x$.

The tire on a vehicle deforms due to the normal load on it and makes contact with the road over a non-zero footprint area called the contact patch (see Figure 13-1 of this book).

First, consider the case where the wheel is a driving wheel, for example, the front wheels in a front-wheel drive vehicle. In this case, since the wheel is a driving wheel, $r_{eff}\omega_w > V_x$. Hence the net velocity of the treads is in a direction opposite to that of the longitudinal velocity of the vehicle. Assume that the slip $r_{eff}\omega_w - V_x$ is small. Then there is a region of the contact patch where the tread elements do not slide with respect to the ground (called the "static region" in Figure 4-3). As the tire rotates and a tread element enters the contact patch, its tip which is in contact with the ground must have zero velocity. This is because there is no sliding in the static region of the contact patch. The top of the tread element moves with a velocity of $R\omega_w - V_x$. Hence the tread element will bend forward as shown in Figure 4-3 and the bending will be in the direction of the longitudinal direction of motion of the vehicle. The maximum bending deflection of the tread is proportional to the slip velocity $r_{eff}\omega_w - V_x$ and to the time duration for which the tread element remains in the contact patch. The time duration in the contact patch is inversely proportional to the rotational velocity $r_{eff}\omega_w$. Hence the maximum

deflection of the tread element is proportional to the ratio of slip to absolute velocity i.e. proportional to the slip ratio $\frac{r_{eff}\omega_w - V_x}{r_{eff}\omega_w}$.

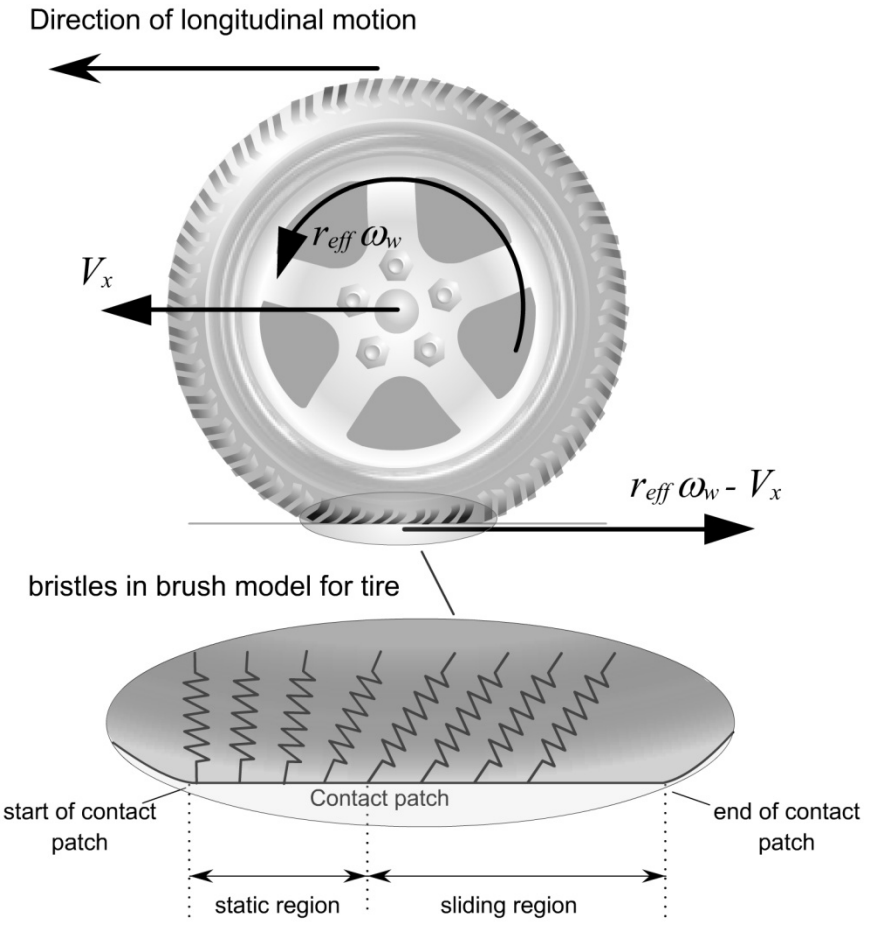

Figure 4-3. Longitudinal force in a driving wheel

Thus the net longitudinal force on the tires from the ground is in the forward direction in the case of a driving wheel and is proportional to the slip ratio of the wheel.

In the case where the tire is on a driven wheel, the longitudinal velocity is greater than the rotational velocity $(V_x > r_{eff}\omega_w)$. In this case the net velocity at the treads is in the forward direction and hence the bristles on the tire will bend backwards. Hence the tire force on the driven wheel is in a

direction opposite to that of the vehicle's longitudinal velocity. Again, for small slip ratio, the tire force will be proportional to slip ratio.

4.1.4 Rolling resistance

As the tire rotates, both the tire and the road are subject to deformation in the contact patch. The road is of course much stiffer and so its deformation can be neglected. But the tire is elastic and new material from the tire continuously enter the contact patch as the tire rotates. Due to the normal load, this material is deflected vertically as it goes through the contact patch and then springs back to its original shape after it leaves the contact patch. Due to the internal damping of the tire material, the energy spent in deforming the tire material is not completely recovered when the material returns to its original shape. This loss of energy can be represented by a force on the tires called the rolling resistance that acts to oppose the motion of the vehicle.

The loss of energy in tire deformation also results in a non-symmetric distribution of the normal tire load over the contact patch. When the tires are static (not rotating), then the distribution of the normal load F_z in the contact patch is symmetric with respect to the center of the contact patch. However, when the tires are rotating, the normal load distribution is non-symmetric, as shown in Figure 4-4.

Imagine the tire being represented by a series of independent springs which resist vertical deformation, as shown in Figure 4-4. As each spring element enters the contact patch, it undergoes vertical deformation. The vertical deformation of the spring reaches its maximum at the center of the contact patch and goes back to zero at the end of the contact patch. If these springs were purely elastic and had no viscous dissipation, then the normal load on the contact patch would be symmetric. But, due to viscous dissipation, the force required to compress the springs in the first half of the contact patch is not fully recovered in the second half of the contact patch. Hence the normal load is not symmetric but is larger in the forward half of the contact patch. This asymmetric normal load distribution is shown in Figure 4-4.

Hence, when the tires are rotating, the resultant normal load F_z moves forward by a distance Δx, as shown in Figure 4-5.

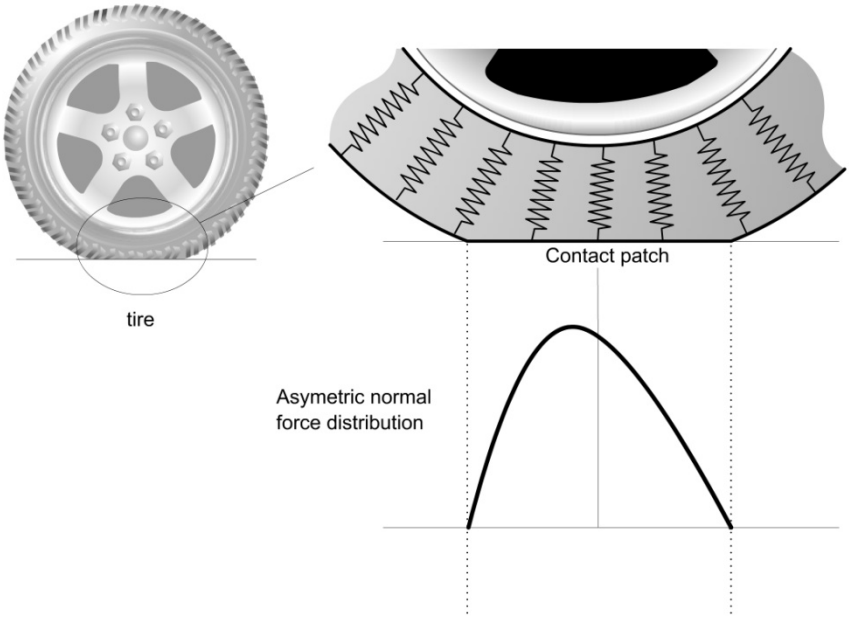

Figure 4-4. Asymmetric normal load distribution on the contact patch

Typically, the rolling resistance is modeled as being roughly proportional to the normal force on each set of tires i.e.

$$R_{xf} + R_{xr} = f(F_{zf} + F_{zr}) \tag{4.15}$$

where f is the rolling resistance coefficient. To see why this approximation is made for the rolling resistance force, consider the action of the normal load and rolling resistance forces shown in Figure 4-5.

The moment $F_z(\Delta x)$ due to the offset normal load is balanced by the moment due to the rolling resistance force $R_x r_{stat}$, where r_{stat} is the statically loaded radius of the tire. Hence

$$R_x = \frac{F_z(\Delta x)}{r_{stat}} \tag{4.16}$$

The variable Δx is not easily measured and therefore R_x is simply modeled as being proportional to F_z with a proportionality constant f.

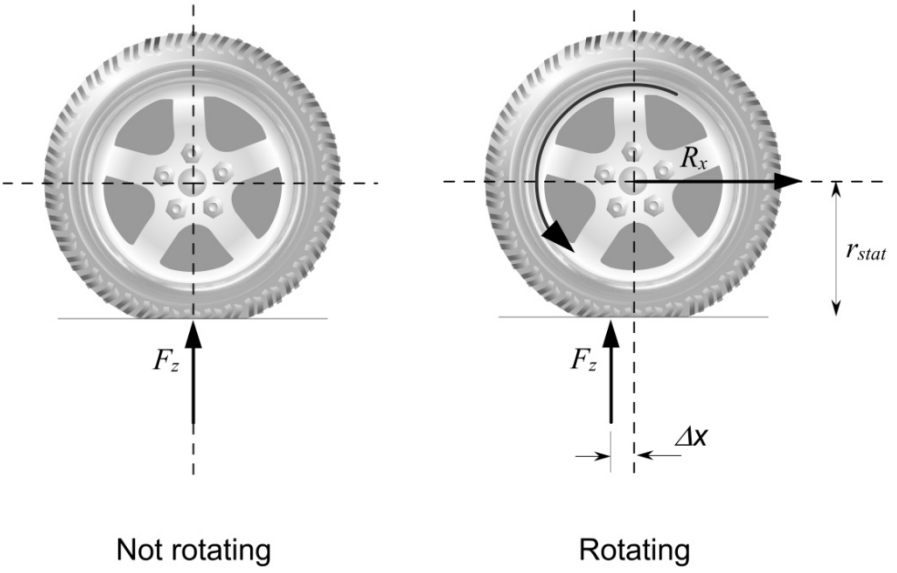

Figure 4-5. Description of rolling resistance

The value of the rolling resistance coefficient f varies in the range 0.01 to 0.04. A value of 0.015 is typical for passenger cars with radial tires (Wong, 2001).

4.1.5 Calculation of normal tire forces

In addition to the total weight of the vehicle, the normal load on the tires is influenced by

a) fore-aft location of the c.g.
b) longitudinal acceleration of the vehicle
c) aerodynamic drag forces on the vehicle
d) grade (inclination) of the road

The normal force distribution on the tires can be determined by assuming that the net pitch torque on the vehicle is zero. In other words, the pitch angle of the vehicle is assumed to have reached a steady state value. Define the following variables

h the height of the c.g. of the vehicle

h_{aero} the height of the location at which the equivalent aerodynamic force acts

ℓ_f the longitudinal distance of the front axle from the c.g. of the vehicle

ℓ_r the longitudinal distance of the rear axle from the c.g. of the vehicle

r_{eff} the effective radius of the tires

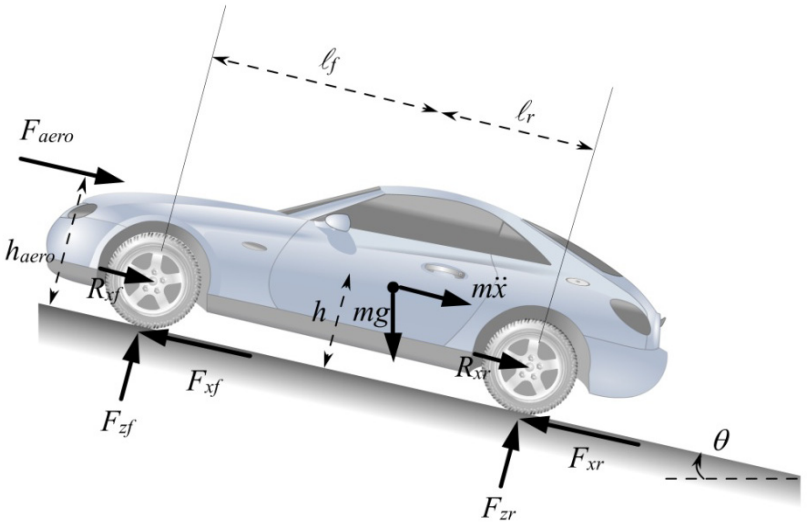

Figure 4-6. Calculation of normal tire loads

Taking moments about the contact point of the rear tire in Figure 4-6

$$F_{zf}(\ell_f + \ell_r) + F_{aero}h_{aero} + m\ddot{x}h + mgh\sin(\theta) - mg\ell_r\cos(\theta) = 0$$

Solving for F_{zf} yields

$$F_{zf} = \frac{-F_{aero}h_{aero} - m\ddot{x}h - mgh\sin(\theta) + mg\ell_r\cos(\theta)}{\ell_f + \ell_r} \tag{4.17}$$

Taking moments about the contact point of the front tire

$$F_{zr}(\ell_f + \ell_r) - F_{aero}h_{aero} - m\ddot{x}h - mgh\sin(\theta) - mg\ell_f\cos(\theta) = 0$$

Solving for F_{zr} yields

$$F_{zr} = \frac{F_{aero}h_{aero} + m\ddot{x}h + mgh\sin(\theta) + mg\ell_f\cos(\theta)}{\ell_f + \ell_r} \tag{4.18}$$

Hence, as the vehicle accelerates, the normal load on the front tires decreases whereas the normal load on the rear tires increases.

4.1.6 Calculation of effective tire radius

The effective tire radius r_{eff} is the value of the radius which relates the rotational angular velocity of the wheel ω_w to the linear longitudinal velocity of the wheel V_{eff} as it moves through the contact patch of the tire with the ground.

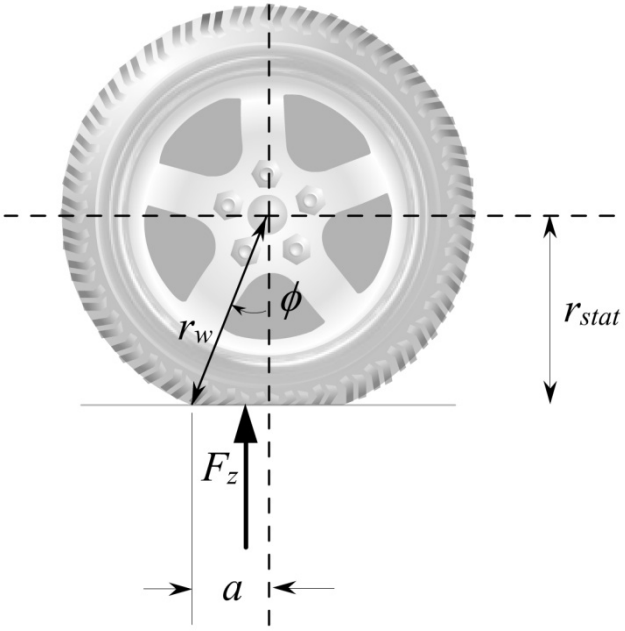

Figure 4-7. Calculation of effective tire radius

If the rotational speed of the wheel is ω_w, the linear equivalent of the rotational speed of the tire is $V_{eff} = r_{eff}\omega_w$ (Kiencke and Nielsen, 2000).

As shown in Figure 4-7, let $2a$ be the longitudinal length of the contact patch and ϕ be the angle made by the radial line joining the center of the wheel to the end of the contact patch. Let t be the duration of time taken by an element of the tire to move through half the contact patch. Then (Kiencke and Nielsen, 2000)

$$V_{eff} = r_{eff}\omega_w = \frac{a}{t} \tag{4.19}$$

At the same time, the rotational speed of the wheel is

$$\omega_w = \frac{\phi}{t} \tag{4.20}$$

Hence

$$r_{eff} = \frac{a}{\phi} \tag{4.21}$$

The static tire radius is the difference between the undeformed radius of the tire r_w and the static vertical deflection of the tire:

$$r_{stat} = r_w - \frac{F_z}{k_t} \tag{4.22}$$

where k_t is the vertical tire stiffness.

From the geometric relationships seen in Figure 4-7

$$r_{stat} = r_w \cos(\phi) \tag{4.23}$$

$$a = r_w \sin(\phi) \tag{4.24}$$

Hence the effective tire radius is given by

$$r_{eff} = \frac{\sin\left\{\cos^{-1}\left(\frac{r_{stat}}{r_w}\right)\right\}}{\cos^{-1}\left(\frac{r_{stat}}{r_w}\right)} r_w \tag{4.25}$$

Note that since $r_{eff} = \frac{\sin(\phi)}{\phi} r_w$, $r_{eff} < r_w$ and that since $r_{eff} = \frac{\tan(\phi)}{\phi} r_{stat}$, $r_{eff} > r_{stat}$. Thus

$$r_{stat} < r_{eff} < r_w \tag{4.26}$$

4.2 DRIVELINE DYNAMICS

In the previous section, we saw that the longitudinal motion equation for the vehicle is of the type

$$m\ddot{x} = F_{xf} + F_{xr} - R_{xf} - R_{xr} - F_{aero} - mg\sin(\theta) \tag{4.27}$$

where F_{xf} and F_{xr} are the longitudinal tire forces. The longitudinal tire forces on the driving wheels are the primary forces that help the vehicle move forward. These forces depend on the difference between the rotational wheel velocity $r_{eff}\omega_w$ and the vehicle longitudinal velocity $\dot{x}$. The wheel rotational velocity ω_w is highly influenced by the driveline dynamics of the vehicle. The major components of a driveline are shown in Figure 4-8 below. The flow of power and the direction of loads on the components is shown in Figure 4-9.

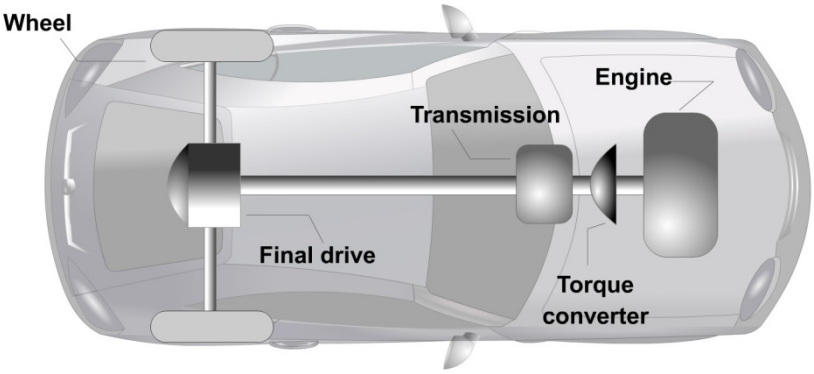

Figure 4-8. Components of a front-wheel drive vehicle powertrain

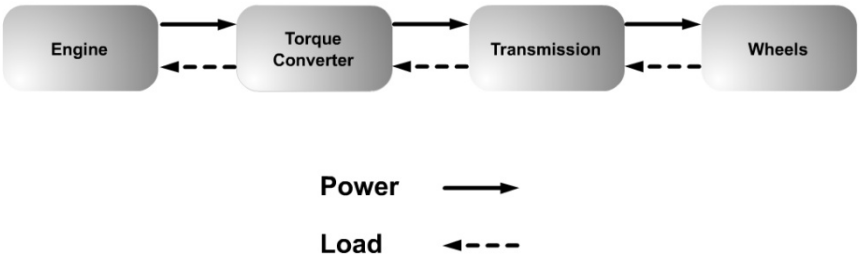

Figure 4-9. Power flow and loads in vehicle drivetrain

4.2.1 Torque converter

The torque converter is a type of fluid coupling that connects the engine to the transmission. If the engine is turning slowly, such as when the car is idling at a stoplight, the amount of torque passed through the torque converter is very small, so keeping the car still requires only a light pressure on the brake pedal.

In addition to allowing the car come to a complete stop without stalling the engine, the torque converter gives the car more torque when it accelerates out of a stop. Modern torque converters can multiply the torque of the engine by two to three times. This effect only happens when the engine is turning much faster than the transmission. At higher speeds, the transmission catches up to the engine, eventually moving at *almost* the same speed. Ideally, though, the transmission should move at exactly the same speed as the engine, because the difference in speed wastes power. To counter this effect, many cars have a torque converter with a lockup clutch. When the two halves of the torque converter get up to speed, this clutch locks them together, eliminating the slippage and improving efficiency.

The torque converter is typically unlocked as soon as the driver removes his/her foot from the accelerator pedal and steps on the brakes. This allows the engine to keep running even if the driver brakes to slow the wheels down.

The major components of the torque converter are a pump, a turbine and the transmission fluid. The fins that make up the pump of the torque converter are attached to the flywheel of the engine. The pump therefore turns at the same speed as the engine. The turbine is connected to the transmission and causes the transmission to spin at the same speed as the turbine, this basically moves the car. The coupling between the turbine and the pump is through the transmission fluid. Torque is transmitted from the pump to the turbine of the torque converter.

Torque converter modeling (both physically based and input-output data based) has been studied by various researchers (see, for example, Kotwicki, 1982, Tugcu, et. al., 1986, Runde, 1986). The static model of Kotwicki (1982) is desirable for control because of its simplicity. It has a reasonable agreement with experimental data for a fairly wide range of operating conditions. This model is a quadratic regression fit of the data from a simple experiment, which involves measuring only the input and output speeds and torques of the torque converter. For the torque converter in Kotwicki (1982), the model expressions are as outlined below.

Let T_p and T_t be pump and turbine torques and $\omega_p (= \omega_e)$ and ω_t be pump and turbine speeds. For converter mode (i.e. $\omega_t / \omega_p < 0.9$), the pump and turbine torques are given by

$$T_p = 3.4325es - 3\omega_p{}^2 + 2.2210\text{x}10^{-3}\omega_p\omega_t - 4.6041\text{x}10^{-3}\omega_t{}^2 \tag{4.28}$$

$$T_t = 5.7656\text{x}10^{-3}\omega_p{}^2 + 0.3107\text{x}10^{-3}\omega_p\omega_t - 5.4323\text{x}10^{-3}\omega_t{}^2 \tag{4.29}$$

For fluid coupling mode (i.e. $\omega_t / \omega_p \geq 0.9$), the pump and turbine torques are given by

$$\begin{aligned} T_p &= T_t \\ &= -6.7644\text{x}10^{-3}\omega_p{}^2 + 32.0024\text{x}10^{-3}\omega_p\omega_t - 25.2441\text{x}10^{-3}\omega_t{}^2 \end{aligned} \tag{4.30}$$

The above equations assume SI units.

The input-output schematic of the torque converter model is shown below in Figure 4-10.

Figure 4-10. Schematic of torque converter model

When the torque converter is locked, as in the third or higher gears, the pump torque is equal to the turbine torque. The pump torque can be calculated in this case by calculating the load on the engine from the wheels and the transmission. This calculation is shown in section 5.5.1.

4.2.2 Transmission dynamics

Let R be the gear ratio of the transmission. The value of R depends on the operating gear and includes the final gear reduction in the differential. In general, $R < 1$ and increases as the gear shifts upwards.

The schematic of the transmission model is shown in Figure 4-11. The turbine torque T_t is the input torque to the transmission. Let the torque transmitted to the wheels be T_{wheels}. At steady state operation under the first, second or higher gears of the transmission, the torque transmitted to the wheels is

$$T_{wheels} = \frac{1}{R} T_t \tag{4.31}$$

The relation between the transmission and wheel speeds is

$$\omega_t = \frac{1}{R} \omega_w \tag{4.32}$$

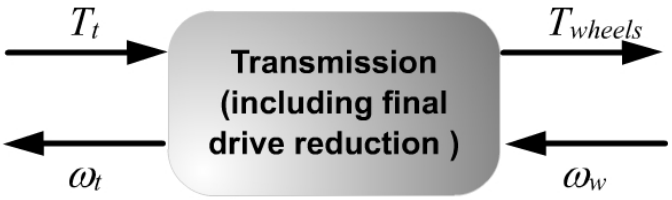

Figure 4-11. Schematic of transmission model

The steady state gear ratio R depends on the operating gear. The operating gear is determined by a gear shift schedule that depends on both the transmission shaft speed and the throttle opening (with fully open throttle angle being counted as 90 degrees). Figure 4-12 shows example up shift and down shift schedules for a 5-speed automatic transmission. Note that the up-shift for each gear change occurs at higher speeds as the throttle angle input from the driver is higher (i.e. the driver is demanding higher torque).

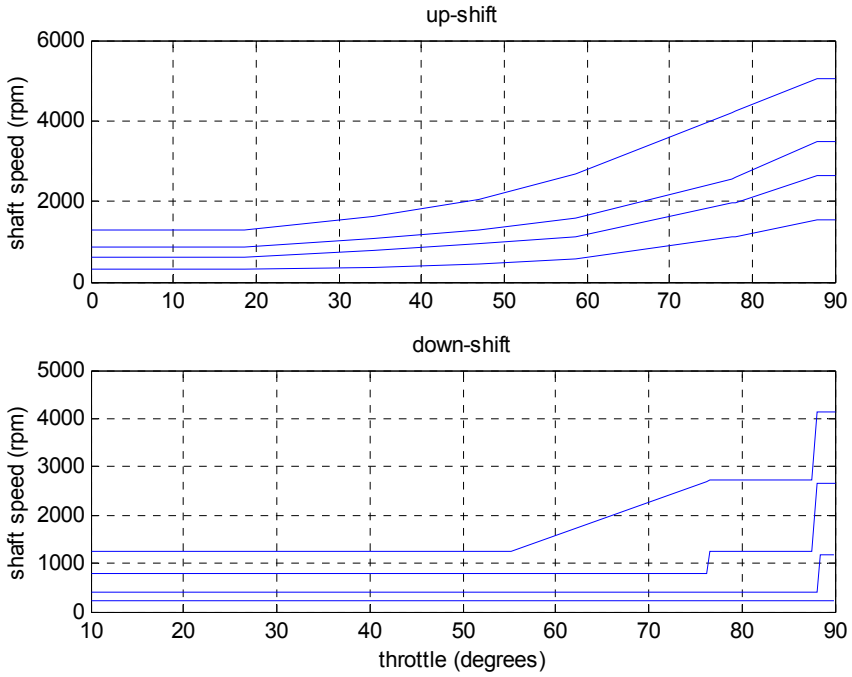

Figure 4-12. Example up shift and down shift schedules for an automatic transmission

Equations describing the dynamics *during* a gear change are complex and can be found in Cho and Hedrick, 1989. An alternative is to replace equations (4.31) and (4.32) by the following 1st order equations *during* a gear change:

$$\tau \dot{T}_{wheel} + T_{wheel} = \frac{1}{R} T_t \tag{4.33}$$

$$\tau \dot{\omega}_t + \omega_t = \frac{\omega_w}{R} \tag{4.34}$$

Equations (4.33) is initialized with $T_{wheel} = 0$ at the instant that the gear change is initiated. R is the gear ratio at the new gear into which the transmission shifts. ω_t is initialized at $\frac{1}{R_{old}} \omega_w$ where R_{old} is the old gear ratio.

The gear change is assumed to be complete when T_{wheel} and ω_t converge to $\frac{1}{R}T_t$ and $\frac{\omega_w}{R}$ within a threshold value. Once the gear change is complete, equations (4.31) and (4.32) can be used again to represent the transmission.

4.2.3 Engine dynamics

The engine rotational speed dynamics can be described by the equation

$$I_e\dot{\omega}_e = T_i - T_f - T_a - T_p \tag{4.35}$$

where T_i is the engine combustion torque, T_f are the torque frictional losses, T_a is the accessory torque and T_p is the pump torque and represents the load on the engine from the torque converter.

Using the notation

$$T_e = T_i - T_f - T_a \tag{4.36}$$

to represent the net engine torque after losses, we have

$$I_e\dot{\omega}_e = T_e - T_p \tag{4.37}$$

The net engine torque T_e depends on the dynamics in the intake and exhaust manifold of the engine and on the accelerator input from the driver. Engine models are discussed in Chapter 9 for both SI and diesel engines and describe how T_e can be calculated. T_p is pump torque and is obtained from equations (4.28) and (4.30) of the torque converter.

The input-output schematic of the engine inertia model is shown in Figure 4-13.

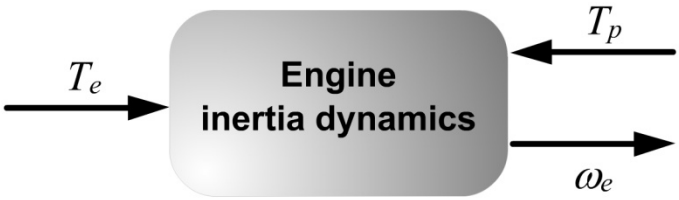

Figure 4-13. Schematic of engine inertia model

4.2.4 Wheel Dynamics

For the driving wheels (for example, the front wheels in a front-wheel driven car), the dynamic equation for the wheel rotational dynamics is

$$I_w \dot{\omega}_{wf} = T_{wheel} - r_{eff} F_{xf} \tag{4.38}$$

where ω_{wf}, T_{wheel} and r_{eff} have been defined earlier and F_{xf} is the longitudinal tire force from the front wheels.

For the non-driven wheels

$$I_w \dot{\omega}_{wr} = -r_{eff} F_{xr} \tag{4.39}$$

where F_{xr} is the longitudinal tire force from the rear wheels.

Figure 4-14. Schematic of wheel dynamics

The total longitudinal tire force is given by

$$F_x = F_{xf} + F_{xr} \tag{4.40}$$

Each of the two tire force terms F_{xf} and F_{xr} is a function of the slip ratio at the front and rear wheels respectively (see section 4.1.2). For

calculation of the slip ratio at the front wheels, ω_{wf} should be used, while for the calculation of the slip ratio at the rear wheels ω_{wr} should be used.

Table 4-1. Summary of longitudinal vehicle dynamic equations

Summary of longitudinal vehicle dynamic equations		
Primary Vehicle Dynamic Equation $m\ddot{x} = F_{xf} + F_{xr} - F_{aero} - R_{xf} - R_{xr} - mg\sin(\theta)$		
1	Front longitudinal tire force	$F_{xf} = C_{\sigma f}\sigma_{xf}$ where $\sigma_{xf} = \frac{r_{eff}\omega_{wf} - \dot{x}}{\dot{x}}$ during braking $\sigma_{xf} = \frac{r_{eff}\omega_{wf} - \dot{x}}{r_{eff}\omega_{wf}}$ during acceleration
2	Rear longitudinal tire force	$F_{xr} = C_{\sigma r}\sigma_{xr}$ where $\sigma_{xr} = \frac{r_{eff}\omega_{wr} - \dot{x}}{\dot{x}}$ during braking $\sigma_{xr} = \frac{r_{eff}\omega_{wr} - \dot{x}}{r_{eff}\omega_{wr}}$ during acceleration
3	Rolling resistance	$R_{xf} + R_{xr} = f(F_{zf} + F_{zr})$ where the front normal tire force is $F_{zf} = \frac{-F_{aero}h_{aero} - m\ddot{x}h - mgh\sin(\theta) + mg\ell_r\cos(\theta)}{\ell_f + \ell_r}$ and the rear normal tire force is $F_{zr} = \frac{F_{aero}h_{aero} + m\ddot{x}h + mgh\sin(\theta) + mg\ell_f\cos(\theta)}{\ell_f + \ell_r}$
4	Aerodynamic drag force	$F_{aero} = \frac{1}{2}\rho C_d A_F(\dot{x} + V_{wind})^2$

4.3 CHAPTER SUMMARY

This chapter presented dynamic equations for the longitudinal motion of the vehicle. The two major elements of the longitudinal dynamic model were the vehicle dynamics and the driveline dynamics.

The vehicle dynamic equations were strongly influenced by longitudinal tire forces, aerodynamic drag forces, rolling resistance forces and gravitational forces. These forces were discussed in detail and mathematical models for each of these forces were described.

The longitudinal driveline system of the vehicle consisted of the internal combustion engine, the torque converter, the transmission and the wheels. Dynamic models for these components were discussed.

NOMENCLATURE

F_{xf}	longitudinal tire force at the front tires
F_{xr}	longitudinal tire force at the rear tires
F_{aero}	equivalent longitudinal aerodynamic drag force
R_{xf}	force due to rolling resistance at the front tires
R_{xr}	force due to rolling resistance at the rear tires
m	mass of the vehicle
g	acceleration due to gravity
θ	angle of inclination of the road on which the vehicle is traveling
ω_w	angular velocity of wheel
r_{eff}	effective radius of rotating tire
r_{stat}	static radius of tire
r_w	radius of undeformed tire
F_z	normal load on tire
Δx	longitudinal distance from center of contact patch at which equivalent normal load acts
a	half-length of contact patch
ϕ	subtended half-angle of contact patch

V_x	longitudinal vehicle velocity
V_{wind}	wind velocity
V_{eff}	effective linear velocity of rotating tire $(=r_{eff}\,\omega_w)$
ρ	mass density of air
C_d	aerodynamic drag coefficient
A_F	frontal area of the vehicle
β	parameter related to aerodynamic drag coefficient calculation
σ_x	slip ratio
h	height of c.g. of vehicle
h_{aero}	height at which equivalent aerodynamic drag force acts
ℓ_f	the longitudinal distance of the front axle from the c.g. of the vehicle
ℓ_r	the longitudinal distance of the rear axle from the c.g. of the vehicle
ω_e	rotational engine speed
ω_t	angular speed of turbine on torque converter
T_p	pump torque
T_t	turbine torque
T_{wheels}	torque transmitted to the wheels
ω_w	angular speed of wheel
τ	time constant in gear change dynamics
R	gear ratio
I_e	engine inertia
T_e	net engine torque after losses
ω_{wf} , ω_{wr}	angular speed of front and rear wheels respectively

REFERENCES

Cho, D. and Hedrick, J.K., "Automotive Powertrain Modeling for Control," *ASME Journal of Dynamic Systems, Measurement and Control*, Vol. 111, pp. 568-576, December 1989.

Dugoff, H., Fancher, P.S. and Segal, L., "Tyre performance charecteristics affecting vehicle response to steering and braking control inputs," *Final Report, Contract CST-460*, Office of Vehicle Systems Research, US National Bureau of Standards, 1969.

Kiencke, U. and Nielsen, L., *Automotive Control Systems for Engine, Driveline and Vehicle*, SAE International, ISBN 0-7680-0505-1, 2000.

Kotwicki, A.J., "Dynamic Models for Torque Converter Equipped Vehicles," *SAE Technical Paper Series*, Paper No. 82039, 1982.

Pacejka, H.B. and Bakker, E., "The Magic Formula Tyre Model," *Vehicle System Dynamics*, v 21, Supplement, Tyre Models for Vehicle Dynamics Analysis, p 1-18, 1993

Pacejka, H.B., "The Tyre as a Vehicle Component," *XXVI FISITA Congress*, Prague, June 16-23, 1996.

Tugcu, A.K., Hebbale, K.V., Alexandridis, A.A., and Karmel, A.M., "Modeling and Simulation of the Powertrain Dynamics of Vehicles Equipped with Automatic Tarnsmission," *Proceedings of the Symposium on Simulation of Ground Vehicles and Transportation Systems*, ASME Winter Annual Meeting, Anaheim, December 1986.

Runde, J., "Modeling and Control of an Automatic Transmission," *S.M.M.E. Thesis*, Department of Mechanical Engineering, M.I.T., January 1986.

White, R.A. and Korst, H.H., "The Determination of Vehicle Drag Contributions from Coastdown Tests," *SAE Transactions*, Vol. 81, paper 720099, 1972.

Wong, J.Y., *Theory of Ground Vehicles*, Wiley-Interscience, ISBN 0-471-35461-9, Third Edition, 2001.

Chapter 5

INTRODUCTION TO LONGITUDINAL CONTROL

5.1 INTRODUCTION

The term "longitudinal controller" is typically used in referring to any control system that controls the longitudinal motion of the vehicle, for example, its longitudinal velocity, acceleration or its longitudinal distance from another preceding vehicle in the same lane on the highway. The throttle and brakes are the actuators used to implement longitudinal control.

A very familiar example of longitudinal control is the standard cruise control system available on most vehicles today. With a standard cruise control system, the driver sets a constant desired speed at which he/she would like the vehicle to travel. The cruise control system then automatically controls the throttle to maintain the desired speed. It is the driver's responsibility to ensure that the vehicle can indeed safely travel at that speed on the highway. If there happens to appear a preceding vehicle on the highway that is traveling at a slower speed or is too close to the ego vehicle, the driver must take action and if necessary apply brakes. Application of the brakes automatically disengages the cruise control system and returns control of the throttle to the driver.

The following examples describe other types of advanced longitudinal control systems.

R. Rajamani, *Vehicle Dynamics and Control*, Mechanical Engineering Series,
DOI 10.1007/978-1-4614-1433-9_5, © Rajesh Rajamani 2012

5.1.1 Adaptive cruise control

An adaptive cruise control (ACC) system is an extension of the standard cruise control system. An ACC equipped vehicle has a radar or other sensor that measures the distance to other preceding vehicles (downstream vehicles) on the highway. In the absence of preceding vehicles, the ACC vehicle travels at a user-set speed, much like a standard cruise controlled vehicle. However, if a preceding vehicle is detected on the highway by the vehicle's radar, the ACC system determines whether or not the vehicle can continue to travel safely at the desired speed. If the preceding vehicle is too close or traveling too slowly, then the ACC system switches from speed control to spacing control (see Figure 5-1). In spacing control, the ACC vehicle controls the throttle and/ or brakes so as to maintain a desired spacing from the preceding vehicle.

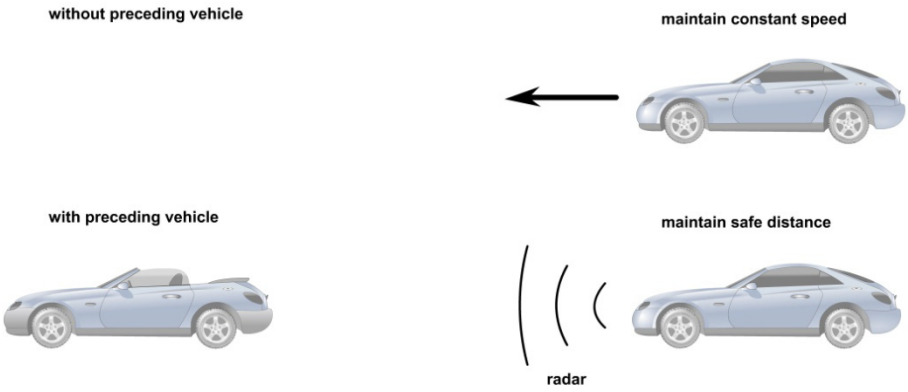

Figure 5-1. Adaptive cruise control

An ACC systems is "autonomous" - it only uses on-board sensors such as radar to accomplish the task of maintaining the desired spacing. It does not depend on wireless communication or on cooperation from other vehicles on the highway. ACC systems were first introduced in Japan (Watanabe, et. al., 1997) and Europe and are now available in the North American market (Fancher, et. al., 1997, Reichart, et. al., 1996 and Woll, 1997). The 2003 Mercedes S-class and E-class passenger sedans come with the option of a radar based Distronic adaptive cruise control system. The 2003 Lexus LS340 comes with an optional laser based adaptive cruise control system.

The design of ACC systems is discussed in detail in Chapter 6.

5.1.2 Collision avoidance

Instead of an ACC system, some vehicles come equipped with a "collision avoidance" (CA) system. A collision avoidance system also operates like a standard cruise control system in the absence of preceding vehicles and maintains a constant desired speed. If a preceding vehicle appears and the CA system determines that the desired speed can no longer be safely maintained, then the CA system reduces the throttle and/or applies brakes so as to slow the vehicle down. In addition, a warning is provided to the driver indicating the presence of other vehicles which necessitate that he or she should take over longitudinal control.

5.1.3 Automated highway systems

A completely different paradigm of longitudinal control is the control of vehicles to travel together in a tightly spaced platoon in automated highway systems (AHS). Automated highway systems have been the subject of intense research and development by several research groups, most notably by the California PATH program at the University of California, Berkeley.

Figure 5-2. Platoon of Buicks used in the NAHSC Demonstration

In an AHS, the objective is to dramatically improve the traffic flow capacity on a highway by enabling vehicles to travel together in tightly spaced platoons. The system requires that only adequately instrumented fully automated vehicles be allowed on this special highway. Manually driven vehicles cannot be allowed to operate on such a highway. Figure 5-2 below shows a photograph of eight fully automated cars traveling together in a tightly spaced platoon during a demonstration conducted by California PATH in August 1997. More details on this experimental demonstration are described in section 7.9. Automated highway systems are the focus of detailed discussion in chapter 7.

5.2 BENEFITS OF LONGITUDINAL AUTOMATION

The development of the longitudinal vehicle control systems described in the previous section has been fueled by a number of motivations, including the desire to enhance driver comfort and convenience, the desire to improve highway safety and the desire to develop solutions to alleviate the traffic congestion on highways.

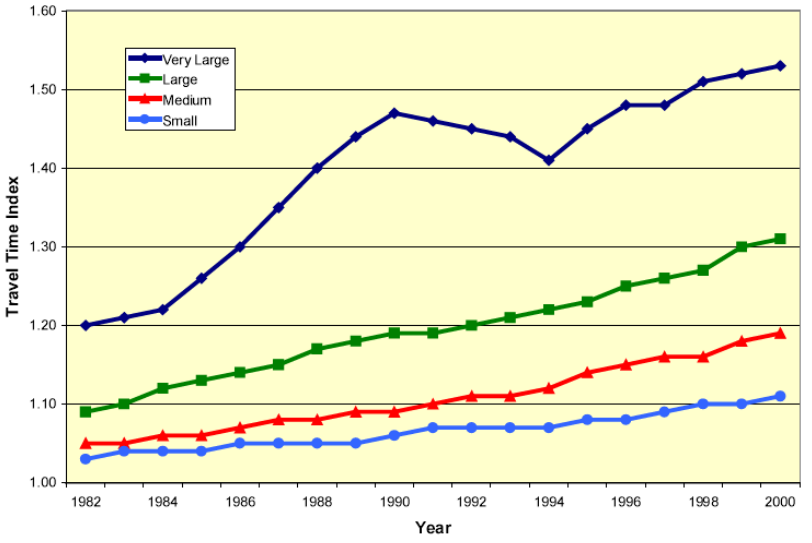

Figure 5-3. Growth in peak period travel time, 1982 to 2000
(Source: Texas Transportation Institute Report, 2002)

An ACC system provides enhanced driver comfort and convenience by allowing extended operation of the cruise control option even in the presence

of other traffic. ACC systems and other automated systems in general are also expected to contribute towards increased safety on the highways. This is because statistics of highway accidents show that over 90% of accidents are caused by human error (United States DOT Report, 1992). Only a very small percentage of accidents are the result of vehicle equipment failure or even due to environmental conditions (like, for example, slippery roads). Since automated systems reduce driver burden and provide driver assistance, it is expected that the use of well-designed automated systems will certainly lead to reduced accidents.

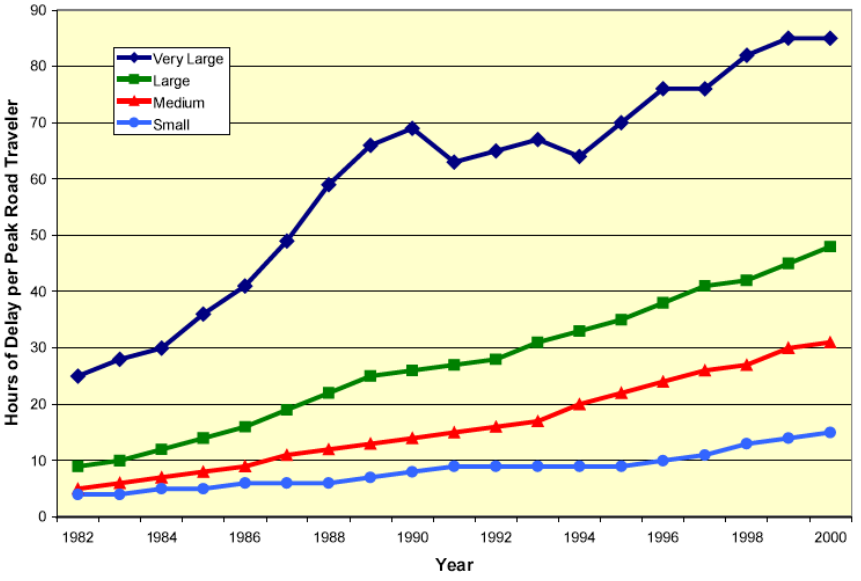

Figure 5-4. Growth in annual delay per peak road traveler, 1982 to 2000
(Source: Texas Transportation Institute Report, 2002)

The development of automated highway systems has been the direct result of the motivation to address traffic congestion on highways. Congestion has been increasing steadily in the country's major metropolitan areas to an extent where two-thirds of all highway travel today is congested travel. Using both the Travel Time Index (Figure 5-3) and annual delay per peak traveler (Figure 5-4), congestion appears to be increasing in cities of all sizes (Texas Transportation Institute Report, 2002). It appears unlikely that the congestion problem will be solved in the foreseeable future by highway expansion. The increase in traffic every year outpaces the increase in capacity due to additional highway construction (Texas Transportation Institute Report, 2002). Thus highway congestion is only expected to worsen every year. The development of AHS is an attempt to use technology to

address the traffic congestion issue. An AHS in which vehicles travel in closely packed platoons can provide a highway capacity that is three times the capacity of a typical highway (Varaiya, 1993).

Having introduced the types of longitudinal control systems under development by various automotive researchers, we next move on to studying the technical details of designing longitudinal control systems.

5.3 CRUISE CONTROL

In a standard cruise control system, the speed of the vehicle is controlled to a desired value using the throttle control input. The longitudinal control system architecture for the cruise control vehicle will be designed to be hierarchical, with an upper level controller and a lower level controller as shown in Figure 5-5.

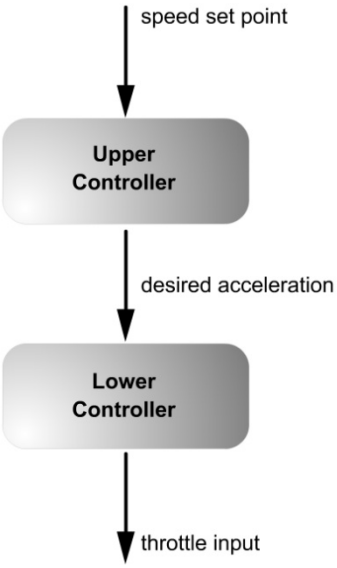

Figure 5-5. Structure of cruise control system

The upper level controller determines the desired acceleration for the vehicle. The lower level controller determines the throttle input required to track the desired acceleration. Vehicle dynamic models, engine maps and nonlinear control synthesis techniques (Choi and Devlin, 1995a and 1995b, Hedrick et al, 1991, Hedrick, et. al., 1993) are used by the lower controller in calculating the real-time throttle input required to track the desired acceleration.

In performance specifications for the design of the upper controller, it is necessary to specify that the steady state tracking error of the controller should be zero. In other words, the speed of the vehicle should converge to the desired speed set by the driver. Other desirable performance specifications might include zero overshoot and adequately fast rise time.

As far as the upper level controller is concerned, the plant model used for control design is

$$\ddot{x} = \frac{1}{\tau s + 1} \ddot{x}_{des} \tag{5.1}$$

or

$$\tau \dddot{x} + \ddot{x} = \ddot{x}_{des} \tag{5.2}$$

where x is the longitudinal position of the vehicle measured from an inertial reference. This means that the upper controller uses desired acceleration as the control input. The actual acceleration of the vehicle is assumed to track the desired acceleration with a time constant τ.

As far as the lower level controller is concerned, the driveline dynamics discussed in chapter 4 and the engine dynamics discussed in chapter 9 constitute the actual longitudinal vehicle model that must be utilized in control design. The lower level controller must ensure that the vehicle acceleration tracks the desired acceleration determined by the upper controller.

Due to the finite bandwidth associated with the lower controller, the vehicle is expected to track its desired acceleration imperfectly. Thus there is a first order lag in the lower level controller performance and hence the use of the model equation (5.1) for the upper controller which incorporates a lag in tracking desired acceleration.

This chapter assumes a lag of $\tau = 0.5$ for analysis and simulation.

5.4 UPPER LEVEL CONTROLLER FOR CRUISE CONTROL

A typical algorithm used for the upper controller is PI control using error in speed as the feedback signal:

$$\ddot{x}_{des}(t) = -k_p\left(V_x - V_{ref}\right) - k_I \int_0^t \left(V_x - V_{ref}\right) dt \tag{5.3}$$

where V_{ref} is the desired vehicle speed set by the user.

Define the following reference position

$$x_{des} = \int_0^t V_{ref}\, d\tau \tag{5.4}$$

Here $x_{des}(t)$ is the position of an imagined reference vehicle that is traveling at the reference or desired speed. Then the upper controller can be rewritten as

$$\ddot{x}_{des} = -k_p\left(\dot{x} - \dot{x}_{des}\right) - k_I\left(x - x_{des}\right) \tag{5.5}$$

This is equivalent to inter-vehicle spacing control with $x - x_{des}$ being the spacing from a fictitious vehicle traveling at the desired reference speed.

The unity feedback loop denoting this closed-loop system is shown below in Figure 5-6.

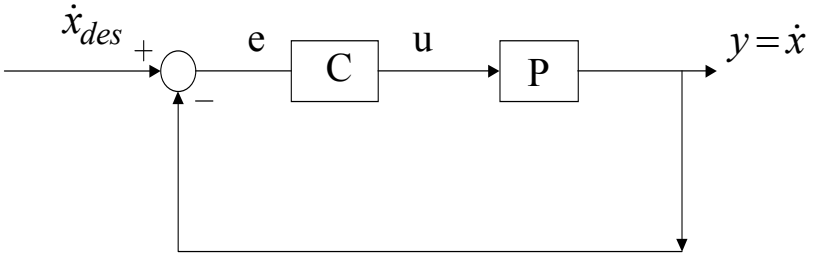

Figure 5-6. Unity feedback loop for upper controller for cruise control

As discussed previously, the plant model for the upper controller is the transfer function between desired acceleration and actual vehicle speed and is given by

$$P(s) = \frac{1}{s(\tau s + 1)} \tag{5.6}$$

The PI controller is

$$C(s) = k_p + \frac{k_i}{s} \tag{5.7}$$

Hence the closed-loop transfer function is

$$\frac{V_x}{V_{ref}} = \frac{PC}{1+PC} = \frac{k_p s + k_i}{\tau s^3 + s^2 + k_p s + k_i} \tag{5.8}$$

A root locus of the feedback system is shown in Figure 5-7 for varying k_p with the ratio $\frac{k_p}{k_i}$ fixed at 4. A value of $\tau = 0.5$ was assumed for the system lag. Values of k_p varying from 0 to 0.75 were used. It can be seen from Figure 5-7 that the closed system is stable for all non-zero k_p. There is one closed-loop real pole and a pair of complex conjugate poles. For a value of k_p = 0.75, the complex poles have a damping ratio of 0.87. If the value of k_p is increased further beyond 0.75, the damping ratio of the complex poles decreases and the system becomes less damped.

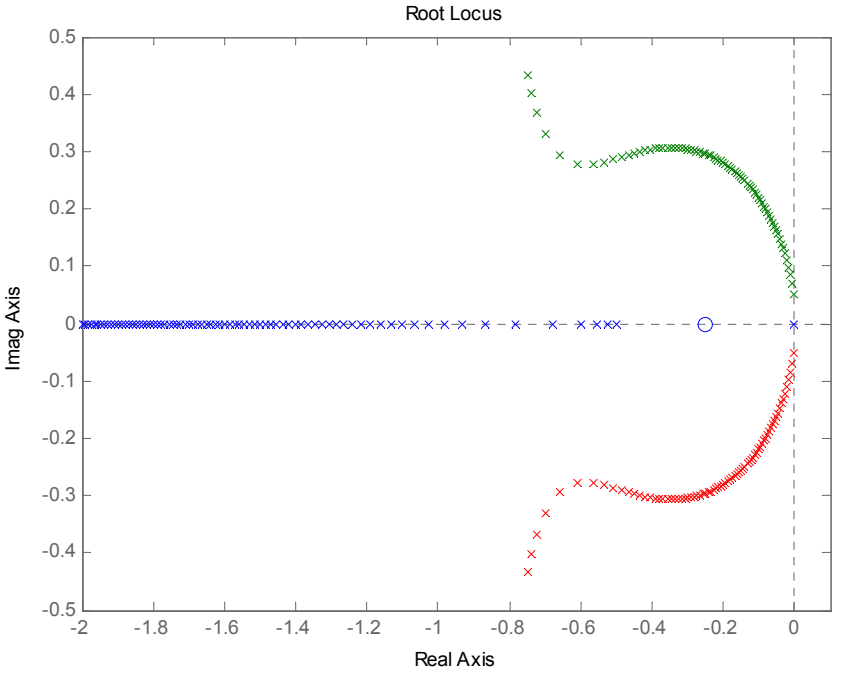

Figure 5-7. Root locus for PI controller

The Bode magnitude plot of the closed-loop transfer function is shown in Figure 5-8 for a value of $k_p = 0.75$. As seen in the figure, the resulting bandwidth of the closed-loop system is 0.2 Hz.

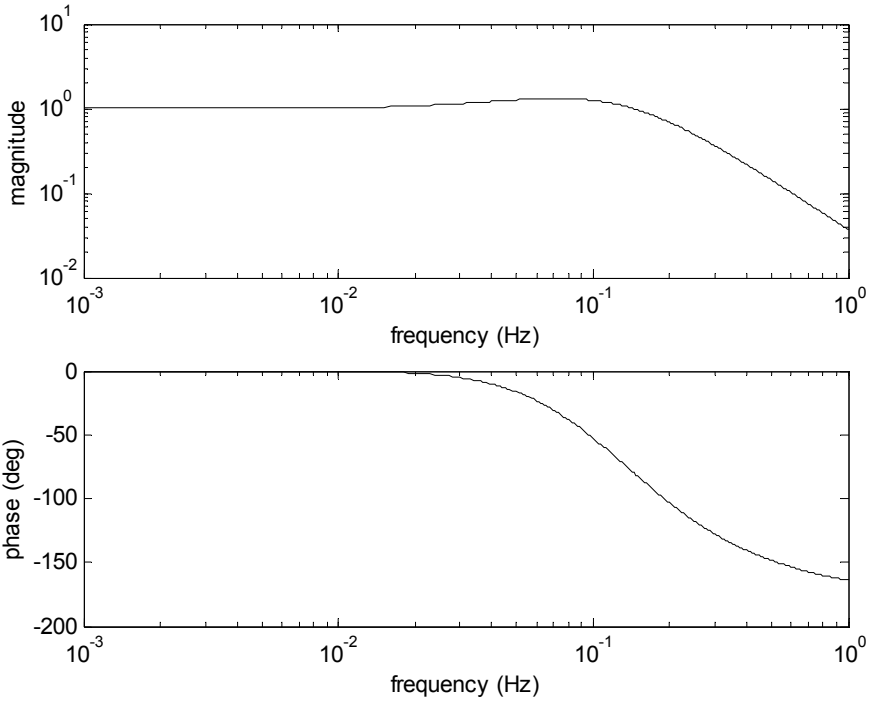

Figure 5-8. Closed-loop transfer function with PI controller

5.5 LOWER LEVEL CONTROLLER FOR CRUISE CONTROL

In the lower controller, the throttle input is calculated so as to track the desired acceleration determined by the upper controller. A simplified model of longitudinal vehicle dynamics can be used in the design of the lower level controller. This simplified model is typically based on the assumptions that the torque converter in the vehicle is locked and that there is zero-slip between the tires and the road (Hedrick, et. al., 1991). These are very reasonable assumptions during cruise control because

a) The cruise control system is typically engaged in gears 3 and higher where the torque converter is indeed locked.

b) The tire slip is small since the longitudinal maneuvers involved in cruise control are very gentle.

Using the above assumptions, the engine torque required to track the desired acceleration command is first calculated. This calculation is described in section 5.5.1. Once the required engine torque has been obtained, engine maps and nonlinear control techniques are used to calculate the throttle input that will provide this required torque.

5.5.1 Engine Torque Calculation for Desired Acceleration

A model of the driveline dynamics was discussed in section 4.2 of this book and should be reviewed by the reader. Consider the case where the torque converter is locked $(T_t = T_p)$, the transmission is in steady state (it is not undergoing a gear shift) and the longitudinal tire slip is negligible. In this case, the wheel speed ω_w is proportional to the engine speed ω_e and related through the gear ratio R as follows

$$\omega_w = R\omega_e \tag{5.9}$$

and the transmission shaft speed is equal to the engine speed

$$\omega_t = \omega_e \tag{5.10}$$

The longitudinal vehicle velocity is approximated by $\dot{x} = r_{eff}\omega_w$ where r_{eff} is the effective tire radius and hence the longitudinal acceleration is

$$\ddot{x} = r_{eff} R\dot{\omega}_e \tag{5.11}$$

The longitudinal vehicle equation is

$$m\ddot{x} = F_x - R_x - F_{aero}$$

where F_x is the total longitudinal tire force from all tires, R_x is the rolling resistance force and F_{aero} is the aerodynamic drag force. Using equation (5.11), this can be rewritten as

$$mRr_{eff}\dot{\omega}_e = F_x - R_x - F_{aero} \tag{5.12}$$

Hence

$$F_x = mRr_{eff}\dot{\omega}_e + R_x + F_{aero} \tag{5.13}$$

Substituting from equation (5.13) into the equation for the wheel rotational dynamics (4.38)

$$I_w\dot{\omega}_w = T_{wheel} - r_{eff}(F_x) = T_{wheel} - mRr_{eff}{}^2\dot{\omega}_e - r_{eff}R_x - r_{eff}F_{aero} \tag{5.14}$$

Hence, the torque at the wheels required to produce the desired acceleration is

$$T_{wheel} = I_wR\dot{\omega}_e + mRr_{eff}{}^2\dot{\omega}_e + r_{eff}F_{aero} + r_{eff}R_x \tag{5.15}$$

Substituting from equation (5.15) into the equation for the transmission dynamics

$$I_t\dot{\omega}_t = T_t - RT_{wheel} = T_t - I_wR^2\dot{\omega}_e - mR^2r_{eff}{}^2\dot{\omega}_e - Rr_{eff}F_{aero} - Rr_{eff}R_x$$

Since $\omega_t = \omega_e$ and $T_t = T_p$, we have

$$I_t\dot{\omega}_e = T_p - I_wR^2\dot{\omega}_e - mR^2r_{eff}{}^2\dot{\omega}_e - Rr_{eff}F_{aero} - Rr_{eff}R_x$$

Hence the pump torque load on the engine is

$$T_p = (I_t + I_wR^2 + mR^2r_{eff}{}^2)\dot{\omega}_e + Rr_{eff}F_{aero} + Rr_{eff}R_x \tag{5.16}$$

Substituting from equation (5.16) into the engine rotational dynamics equation (4.35)

$$I_e\dot{\omega}_e = T_{net} - T_p$$
$$= T_{net} - (I_t + I_wR^2 + mR^2r_{eff}{}^2)\dot{\omega}_e - Rr_{eff}F_{aero} - Rr_{eff}R_x$$

Hence

$$I_e\dot{\omega}_e = T_{net} - (I_t + I_wR^2 + mR^2r_{eff}{}^2)\dot{\omega}_e - Rr_{eff}F_{aero} - Rr_{eff}R_x$$

or

$$J_e\dot{\omega}_e = T_{net} - Rr_{eff}F_{aero} - Rr_{eff}R_x \tag{5.17}$$

where

$$J_e = I_e + I_t + R^2 I_w + mR^2 {r_{eff}}^2 \tag{5.18}$$

Since F_{aero} is a quadratic function of vehicle velocity and can also be expressed in terms of a quadratic in ω_e, equation (5.16) represents a single first order o.d.e. that describes the vehicle dynamics in the case where the torque converter is locked and the slip is assumed to be negligible.

Substituting for F_{aero} as $F_{aero} = c_a\left(r_{eff}R\omega_e\right)^2$, the dynamics relating engine speed ω_e to the pseudo-input "net combustion torque" T_{net} can be modeled by the single first-order ode

$$\dot{\omega}_e = \frac{T_{net} - c_a R^3 {r_{eff}}^3 {\omega_e}^2 - R(r_{eff}R_x)}{J_e} \tag{5.19}$$

where $J_e = I_e + I_t + (m{r_{eff}}^2 + I_\omega)R^2$ is the effective inertia reflected on the engine side.

From equation (5.19), it is clear that if the net combustion torque is chosen as

$$(T_{net}) = \frac{J_e}{R\, r_{eff}}\ddot{x}_{des} + [c_a R^3 {r_{eff}}^3 {\omega_e}^2 + R(r_{eff}R_x)] \tag{5.20}$$

then the acceleration of the car is equal to the desired acceleration defined by the upper level controller i.e. $\ddot{x} = \ddot{x}_{des}$.

5.5.2 Engine Control

Once the required combustion torque is obtained from (5.20), the control law to calculate the throttle angle to provide this torque can be obtained by using engine dynamic models and applying nonlinear control synthesis techniques. Engine dynamic models for both SI and diesel engines and nonlinear control design to provide a desired engine torque are discussed in Chapter 9 of this book.

5.6 ANTI-LOCK BRAKE SYSTEMS

5.6.1 Motivation

Anti-lock brake systems (ABS) were originally developed to prevent wheels from locking up during hard braking. Modern ABS systems not only try to prevent wheels from locking but also try to maximize the braking forces generated by the tires by preventing the longitudinal slip ratio from exceeding an optimum value.

First, note that locking of the wheels reduces the braking forces generated by the tires and results in the vehicle taking a longer time to come to a stop. Further, locking of the front wheels prevents the driver from being able to steer the vehicle while it is coming to a stop.

To understand the influence of longitudinal slip ratio on braking forces, consider the tire force characteristics shown in Figure 5-9. As seen in Figure 5-9, the magnitude of the tire longitudinal force typically increases linearly with slip ratio for small slip ratios. It reaches a maximum (peak) value typically at a slip ratio value between 0.1 and 0.15. At slip ratios beyond this value, the magnitude of tire force decreases and levels out to a constant value.

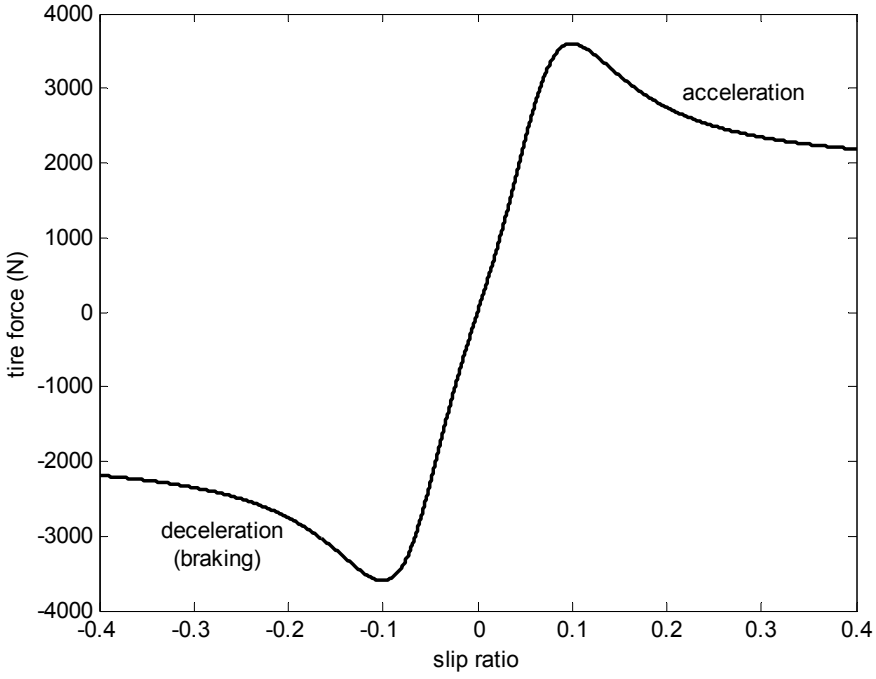

Figure 5-9. Tire longitudinal force as a function of longitudinal slip ratio

If the driver presses hard on the brakes, the wheels will slow down considerably faster than the vehicle slows down, resulting in a big slip ratio value. However, as described above, slip ratios higher than an optimum value actually result in reduced braking forces. The vehicle would take longer to come to a stop if the slip ratio exceeded the optimum value. The ABS solution then is to prevent excessive brake torque from being applied on the wheels, so that the slip ratio doesn't exceed the optimum value. This would also prevent or delay the wheels from locking up and increase steerability of the vehicle during braking.

The following simulation plots demonstrate the negative consequences of very hard braking. Figures 5-10 and 5-11 show vehicle speed and slip ratio respectively during hard braking. As seen in Figure 5-11, the wheels lock during braking and result in a slip value of –1 within 1 second of the initiation of braking. As seen in Figure 5-10, while the wheels come to a stop in 1 second, the vehicle itself does not come to a stop and only reduces in speed from 30 m/s to 13 m/s in 12 seconds.

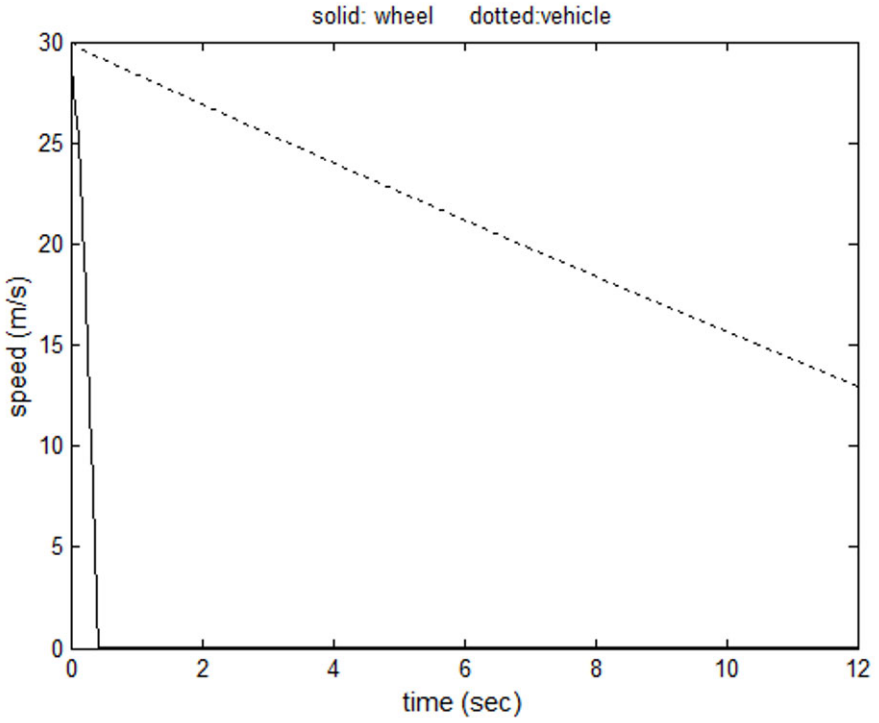

Figure 5-10. Vehicle speed during hard braking (No ABS)

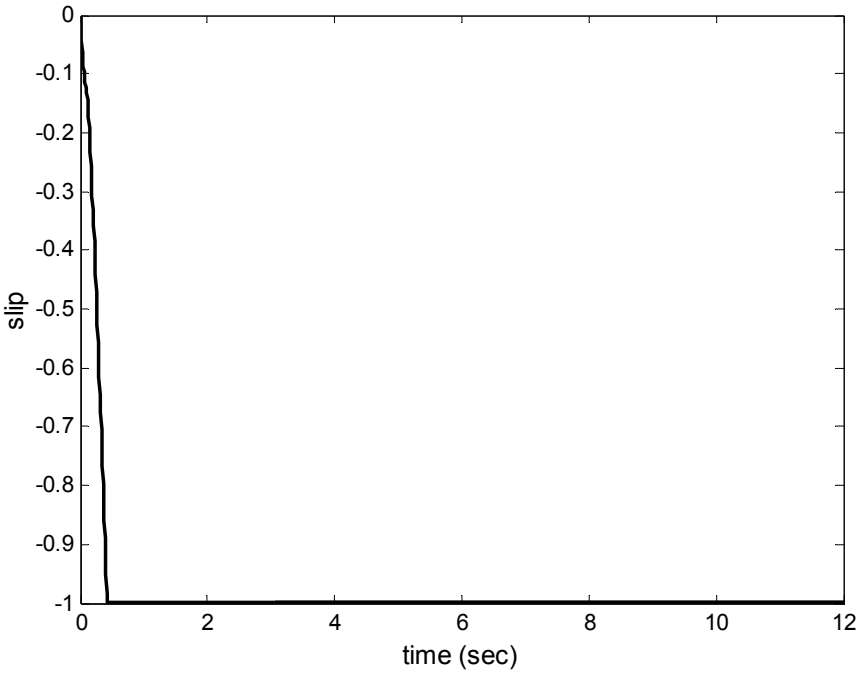

Figure 5-11. Slip Ratio during hard braking (No ABS)

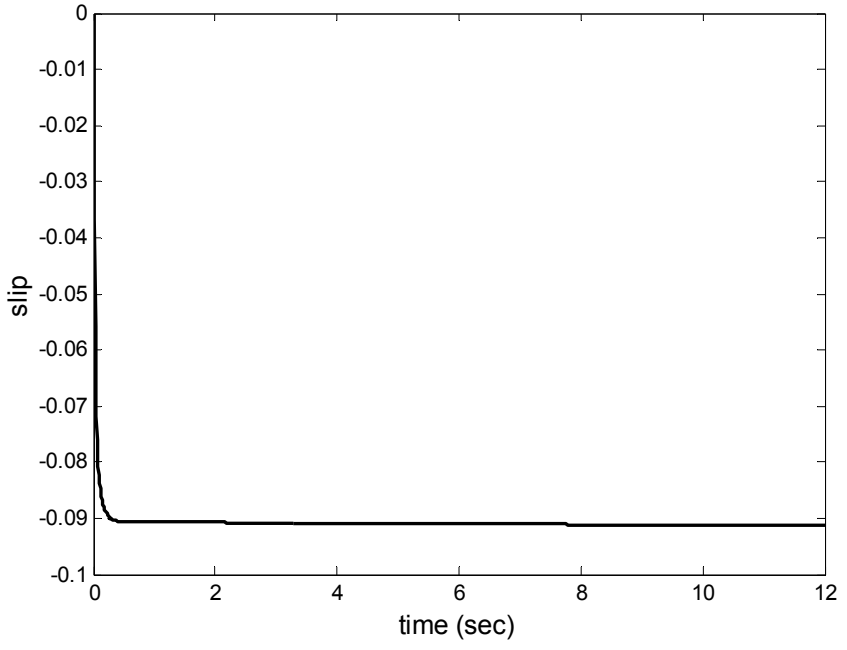

Figure 5-12. Slip Ratio with reduced braking (ABS)

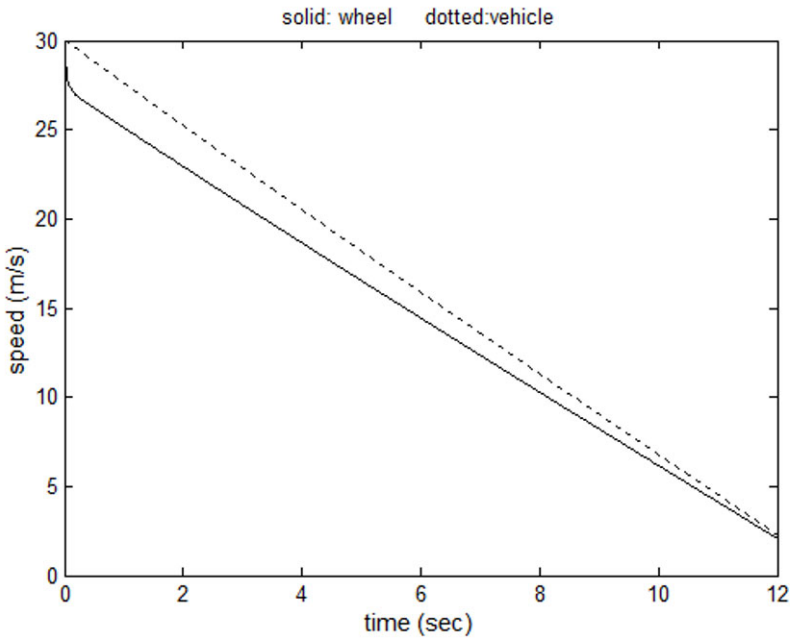

Figure 5-13. Vehicle speed with reduced braking (ABS)

Figures 5-12 and 5-13 show slip ratio and vehicle speed during *reduced braking* designed to just prevent the wheels from locking up. As seen in Figure 5-12, the slip ratio is maintained at 0.09 which is close to the optimum value of 0.1. The wheels don't lock, as seen in Figure 5-13, thus allowing the vehicle to be steered. Further, the speed of the vehicle is reduced from 30 m/s to 2 m/s in 12 seconds. Thus a significantly greater reduction in vehicle speed is obtained by limiting the amount of braking torque applied to the wheels.

5.6.2 ABS Functions

The basic objective of the ABS is to either hold or release the braking pressure on the wheels if there is a danger of the wheels locking. At the same time, the ABS needs to re-permit application of the brakes again once the danger of locking has been averted. The ABS system could also hold or release the braking pressure in order to keep the slip ratio at the wheel from exceeding an optimum value.

Depending on the number of wheels the ABS controls, ABS can be four channel four sensor, three channel three sensor or one channel one sensor. Each channel controlled by the ABS has a valve. Depending on the position of the valve, brake pressure on the wheel is held, released or controlled by the driver:

When the valve is open, pressure from the master cylinder is passed right through to the brake. This allows the brake to be controlled by the driver, allowing the amount of brake pressure desired by the driver to be applied to the brake.

When the valve is closed or blocked, that brake is isolated from the master cylinder. This holds the brake pressure and prevents it from increasing even if the driver pushes the brake pedal harder.

When the valve is in the release position, the pressure from the brake is released. In this position, not only is the brake isolated from any further braking actions of the driver, but the amount of braking pressure on the wheel is actively reduced.

A major practical problem in ABS systems is that wheel slip cannot be measured with inexpensive sensors on a passenger vehicle. Often the only measurements available to the ABS system are measurements of the individual wheel speeds at the four wheels. Algorithms that utilize these wheel speed measurements to predict if the wheels will lock and to predict if the danger of locking has been averted have to be used.

The process of determining whether or not the wheel is going to lock is called *prediction*. Prediction point slip is defined as the wheel slip at the instant the control unit predicts for the first time in a brake cycle that the wheel is going to lock.

The process of determining whether or not the danger of locking has been averted is called *reselection*. Reselection point slip is defined as the wheel slip at the instant it is predicted for the first time in a brake cycle that the danger of locking is averted.

5.6.3 Deceleration Threshold Based Algorithms

One of the most common ABS algorithms is the deceleration threshold based algorithm (Bosch Automotive Handbook, 2000). The wheel deceleration signal is used to predict if the wheel is about to lock. Here wheel deceleration is defined as angular deceleration multiplied by effective tire radius.

A common version of the deceleration threshold algorithm is summarized in Figures 5-14, 5-15, 5-16 and 5-17 (Kiencke and Nielsen, 2000 and Bosch Automotive Handbook, 2000).

Let $\dot{V}_R$ be the wheel deceleration defined as

$$\dot{V}_R = r_{eff}\dot{\omega}_w \tag{5.21}$$

where r_{eff} is the effective tire radius and ω_w is the angular wheel speed. Let a_1, a_2, a_3 and a_4 be acceleration threshold values, all defined to be positive with $a_2 > a_1$ and $a_4 > a_3$.

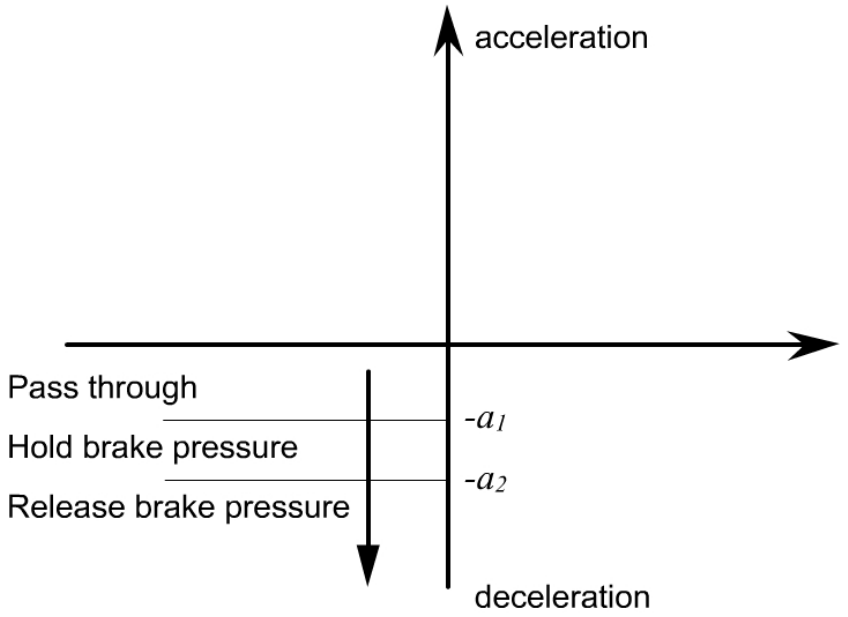

Figure 5-14. Deceleration in the first cycle

When the driver presses on the brake pedal, if the deceleration is less than a_1 (i.e. if $\dot{v}_R > -a_1$), then the driver's braking action is directly passed through to the brakes. When the deceleration exceeds a_1 for the first time (i.e $\dot{v}_R < -a_1$), the driver's braking action is no longer directly passed through to the brakes. Instead the braking pressure is held constant at the pressure value achieved when the deceleration first exceeded a_1. If the wheel deceleration continues to increase further and exceeds the value a_2 (i.e. $\dot{v}_R < -a_2$), then the braking pressure at the wheel is decreased. This will prevent the wheel from decelerating any further and could eventually result in the wheel gaining speed or accelerating. If the wheel deceleration reduces to the value a_2 (i.e. $\dot{v}_R > -a_2$), then the pressure drop is stopped. If the wheel deceleration drops below the value a_1 (i.e. $\dot{v}_R > -a_1$), then the driver's braking action is once again directly passed through to the brakes. If

the wheel actually starts accelerating, and the acceleration exceeds the relatively high threshold a_4, then the braking pressure is actually increased beyond that dictated by the driver's actions, so as to prevent the wheel from over acceleration. In this case, when the wheel's acceleration drops to the value below a_3 (i.e. $\dot{v}_R < a_3$), the driver's braking action are again passed through to the brakes. When the wheel deceleration goes below a_1 ($\dot{v}_R < -a_1$) again the second cycle starts. Running through such cycles, the wheels are prevented from locking and the wheel rotational speed is kept in an area where wheel slip is close to that of the maximum friction coefficient. Note that a_4 is a relatively high deceleration level. (much larger than a_3).

During the second braking cycle, the braking pressure is reduced right away when the deceleration first exceeds a_1 (i.e. the phase of holding brake pressure constant between a_1 and a_2 is no longer done during the second braking cycle). In the first cycle, the short pressure holding phase is used for the filtering of disturbances.

Figure 5-14 and Figure 5-15 summarize the deceleration threshold based algorithm during wheel deceleration. Figure 5-16 and Figure 5-17 summarize the algorithm during wheel acceleration.

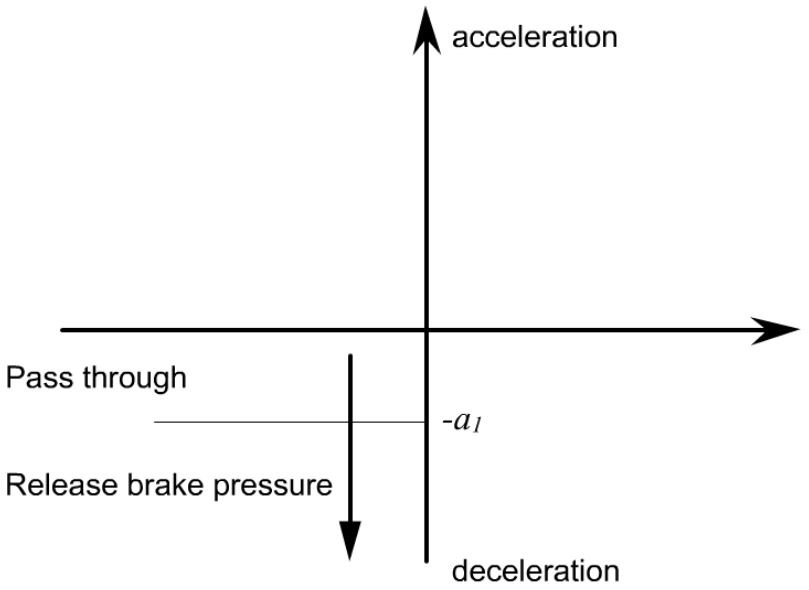

Figure 5-15. Deceleration in the second and subsequent cycles

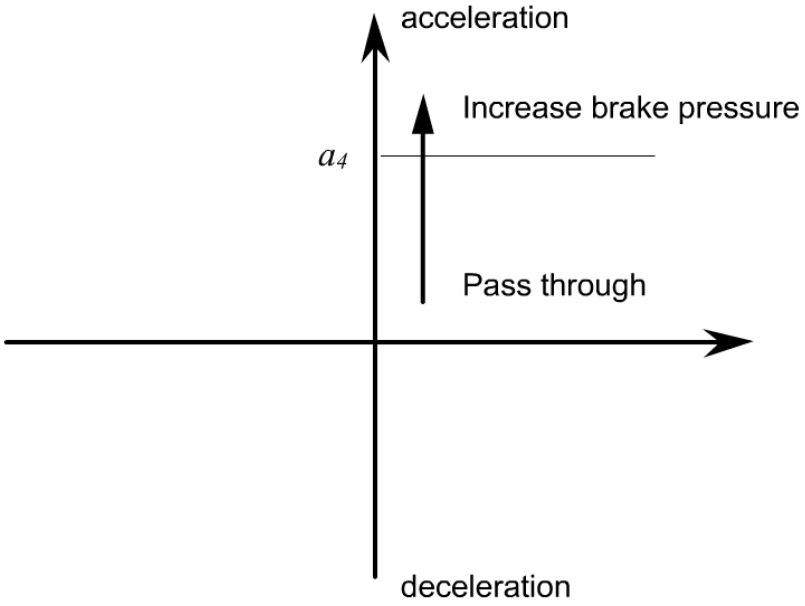

Figure 5-16. Increasing acceleration

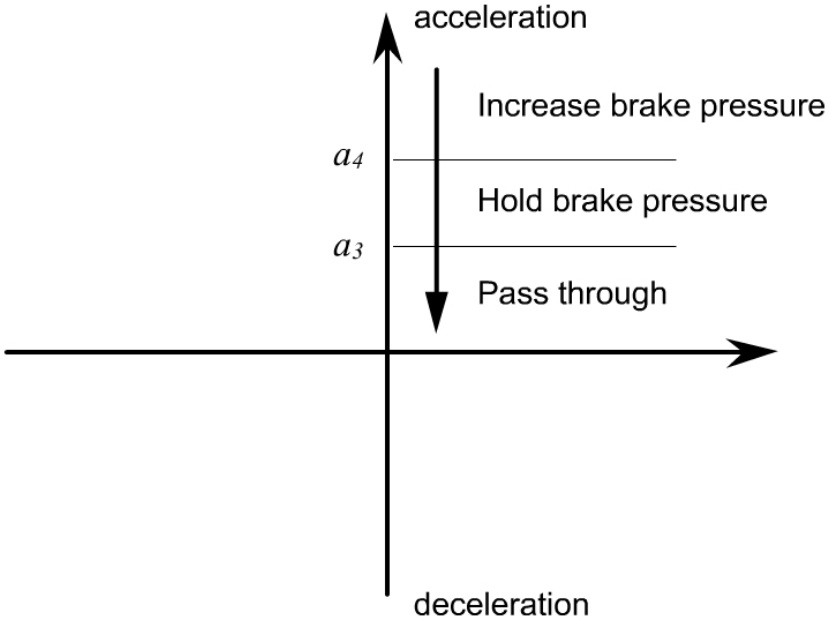

Figure 5-17. Decreasing acceleration

In a modified version of this algorithm, during the first cycle, if the deceleration exceeds a_1 and the wheel speed falls below a slip-switching threshold (determined based on the initial speed when braking first started), then the braking pressure is reduced. Thus the deceleration threshold a_2 is not used in this modified algorithm. From the second braking cycle onwards, pressure is reduced right away when the deceleration first exceeds a_1 (Bosch Automotive Handbook, 2000).

5.6.4 Other Logic Based ABS Control Systems

A number of factors influence the working of the ABS system. These include

The value of the tire-road friction coefficient, since it influences the range within which the wheel slip ratio should be maintained.

The rate of application of the brake torque (brake dynamics). During the first cycle, this depends on how the driver of the vehicle presses the brake pedal. In the subsequent cycles, it depends on the pressure build characteristics of the modulator.

Initial longitudinal velocity of the vehicle is also important, since it determines how quickly the vehicle can come to a stop.

The brake effort distribution from front to rear is also important

The performance of the ABS system for variations in the above parameters is an important consideration in ABS system design. Many logic based ABS control systems have been developed and reported in literature to address performance in the presence of the above variations.

The work by Guntur and Ouwerkerk, 1972 contains a good discussion of logic based ABS system design. It compares different logic controllers by evaluating their performance in simulations based on a mathematical vehicle model. In the simulations the authors vary three important parameters: rate of application of the brake, tire-road friction coefficients (i.e. different road conditions) and initial velocity of the vehicle. Different logic controllers are compared on the basis that, for variations in these parameters, the control unit should

1. Not fail to indicate locking of the wheel
2. Not make false predictions about locking of the wheel
3. Maintain the wheel slip within the desired range

Four different algorithms are evaluated in terms of their prediction of wheel lock. Based on their simulations results, the authors conclude that a compound condition consisting of two algorithms A_p and B_p results in the best performance (Guntur and Ouwerkerk, 1972). Method A_p sets a

maximum threshold deceleration on the wheel speed, while method B_p sets another maximum threshold on the ratio of the deceleration of the wheel speed to the angular wheel speed. In the proposed compound condition, provision is made for an adaptive feature that changes the threshold values for initial velocities exceeding 35 m/s. For initial velocities lower than 35 m/s, a static threshold algorithm is found to be adequate. In considering the suitability of methods for the prediction point, the authors allow locking of the rear wheels as long as it does not cause instability of the vehicle.

Eight different algorithms are evaluated in the same paper in terms of their identification of the reselection point (Guntur and Ouwerkerk, 1972). The authors found that a compound condition consisting of methods A_r, D_r and F_r gives a good estimation of the reselection point. Method A_r is a fixed time delay condition which ensures the reapplication of the brake after a certain fixed time lapse after each time the brake is released. Method D_r is a variable condition on the desired angular velocity. The angular velocity of the wheel at the point of initial braking in the first cycle, or the corresponding signal at the point of reapplication in a subsequent cycle, is stored and the desired angular velocity is assumed to be proportional to this value. This method is used to ensure that the driver of the vehicle can conveniently influence the performance of the anti-skid system by interrupting a given braking maneuver. Method F_r reapplies the brakes whenever a threshold on the ratio of the deceleration of the wheel speed to the angular wheel speed is exceeded. It is added to improve the braking effectiveness at low vehicle speed, and also render the anti-skid system inoperative at very low speed. The compound reselection condition devised by the authors does not incorporate an adaptive feature like the one used for the prediction point condition.

5.6.5 Recent Research Publications on ABS

The development of ABS algorithms continues be an active area of research. Many research papers have concentrated on the development of algorithms that can ensure that a desired wheel slip ratio is tracked at the wheels. Detailed dynamic models of the wheel, tire, vehicle and the hydraulic system are used and the resulting system model is nonlinear. Nonlinear control system techniques are often used to ensure tracking of a desired wheel slip ratio. The measurable states of the system are the hydraulic pressure and the wheel speed. The fact that the vehicle absolute velocity cannot be measured

means that the slip ratio itself cannot be measured. It must be estimated from a observer and this constitutes a very challenging problem. Accounting for changes in road surface conditions in the dynamic tire model (e.g. low friction coefficient on a slippery road) is an additional difficulty. Interesting research papers in this area include Unsal and Kachroo (1999) and Drakunov, et. al. (1995).

5.7 CHAPTER SUMMARY

This chapter provided an introduction to several longitudinal control systems, including standard cruise control, adaptive cruise control, collision avoidance, longitudinal control for operation of vehicles in platoons and anti lock brake systems. Control system design for standard cruise control and anti lock brake systems were discussed in detail. Chapter 6 will next provide a detailed discussion of adaptive cruise control while Chapter 7 will discuss longitudinal control for operation of vehicles in platoons.

NOMENCLATURE

x	longitudinal position of the vehicle from an inertial reference
$\dot{x}$ or V_x	longitudinal velocity of the vehicle
x_{des}	imaginary longitudinal position of a vehicle traveling with the reference speed
$\dot{x}_{ref}$ or V_{ref}	desired vehicle speed set by the driver
k_p, k_i	gains used in PI controller for cruise control
τ	time constant for lag in tracking desired acceleration
T_{net}	net combustion torque of the engine
T_{br}	brake torque
T_{wheel}	torque to the drive wheels
T_p	pump torque
ω_e	engine angular speed
ω_w	wheel angular speed

ω_t	turbine angular speed
c_a	aerodynamic drag coefficient
R	gear ratio
r_{eff}	effective tire radius
R_x	rolling resistance of the tires
F_x	total longitudinal tire force
F_{aero}	aerodynamic drag force
I_e	engine moment of inertia
I_t	transmission shaft moment of inertia
I_w	wheel moment of inertia
I_e	engine moment of inertia
J_e	effective inertia reflected on the engine side
m	vehicle mass
V_R	equivalent linear velocity of rotating wheel
a_1, a_2, a_3, a_4	acceleration thresholds used in ABS algorithm

REFERENCES

Austin, L. and Morrey, D., "Recent Advances in Antilock Braking Systems and Traction Control Systems," *Proceedings of the Institution of Mechanical Engineers,* Vol. 214, pp. 625-638, 2000.

Bosch Automotive Handbook, 5th Edition, ISBN 0-8376-0614-4, Robert Bosch GmbH, 2000.

Chandler, K.N., "Theoretical Studies in Braking," *Proceedings of the Institution of Mechanical Engineers* , 1960-61, No. 4, 147.

Cho, D. and Hedrick, J.K., "Automotive powertrain modeling for control," *ASME Journal of Dynamic Systems, Measurement and Control, Transactions*, v 111, n 4, p 568-576, Dec, 1989.

Choi, S.B. and Hedrick, J.K., "Vehicle Longitudinal Control Using an Adaptive Observer for Automated Highway Systems", *Proceedings of American Control Conference*, Seattle, Washington, 1995.

Choi, S.B. and Devlin, P., "Throttle and Brake Combined Control for Intelligent Vehicle Highway Systems", *SAE 951897*, 1995.

Decker, H., Emig, R. and Goebels, H., "Antilock Brake Systems for Commercial Vehicles," *Proceedings – Society of Automotive Engineers*, 1990, P-233, pp. 515-523.

Drakunov, S., Ozguner, U, Dix, P and Ashrafi, B., "ABS Control using Optimum Search via Sliding Modes," *IEEE Transactions on Control Systems Technology*, Vol. 3, No. 1, pp. 79-85, March 1995.

Fancher, P., Ervin, R., Sayer, J., Hagan, M., Bogard, S., Bareket, Z., Mefford, M. and Haugen, J., 1997, "Intelligent Cruise Control Field Operational test (Interim Report)", *University of Michigan Transportation Research Institute Report,* No. UMTRI-97-11, August 1997.

Guntur, R.R., Ouwerkerk, H., "Adaptive Brake Control System," *Ph.D. Thesis*, Delft University of Technology, The Netherlands, June 1975.

Guntur, R.R. and Wong, J.Y., "Some Design Aspects of Anti-Lock Brake Systems for Commercial Vehicles," *Vehicle System Dynamics*, Vol. 9, pp. 149-180, 1980.

Guntur, R.R. and Ouwerkerk, H., "Adaptive Brake Control System," *Proceedings of the Institution of Mechanical Engineers*, Vol. 186, 68/72, pp. 855-880, 1972.

Hedrick, J.K., McMahon, D., Narendran, V.K. and Swaroop, D., "Longitudinal Vehicle Controller Design for IVHS Systems", *Proceedings of the 1991 American Control Conference*, Vol. 3, pp. 3107-3112, June 1991.

Hedrick, J.K., McMahon, D. and Swaroop, D., "Vehicle Modeling and Control for Automated Highway Systems", *PATH Research Report*, UCB-ITS-PRR-93-24, 1993.

Hedrick, J K. Tomizuka, M. Varaiya, P, "Control Issues in Automated Highway Systems," *IEEE Control Systems Magazine. v 14 n 6, . p 21-32 , Dec 1994*

Ioannou, P.A. and Chien, C.C., 1993, "Autonomous Intelligent Cruise Control", *IEEE Transactions on Vehicular Technology*, Vol. 42, No. 4, pp. 657-672.

Kiencke, U. and Nielsen, L., *Automotive Control Systems for Engine, Driveline and Vehicle*, SAE International, ISBN 0-7680-0505-1, 2000.

Miyasaki, N., Fukumoto, M., Sogo, Y. and Tsukinoki, H., "Antilock Brake System (M-ABS) Based on the Friction Coefficient Between the Wheel and the Road Surface," *SAE Special Publications*, Feb 1990, pp. 101-110.

Nouillant, C., Assadian, F., Moreau, X. and Oustaloup, A., "Feedforward and Crone Feedback Control Strategies for Automobile ABS," *Vehicle System Dynamics*, 2002, Vol. 38, No. 4, pp. 293-315.

Rajamani, R., Tan, H.S., Law, B. and Zhang, W.B., "Demonstration of Integrated Lateral and Longitudinal Control for the Operation of Automated Vehicles in Platoons," *IEEE Transactions on Control Systems Technology*, Vol. 8, No. 4, pp. 695-708, July 2000.

Reichart, G., Haller, G. and Naab, K, 1996, "Driver Assistance : BMW Solutions for the Future of Individual Mobility", *Proceedings of ITS World Congress*, Orlando, October 1996.

Slotine, J.J.E. and Li, W., "Applied Nonlinear Control", Prentice Hall, 1991.

Sugai, M., Yamaguchi, H., Miyashita, M., Umeno, T. and Asano, K., "New Control Technique for Maximizing Braking Force on Antilock Brake System," *Vehicle System Dynamics*, 1999, Vol. 32, pp. 299-312.

Swaroop, D., Hedrick, J.K., Chien, C.C. and Ioannou, P. "A Comparison of Spacing and Headway Control Laws for Automatically Controlled Vehicles", *Vehicle System Dynamics Journal*, Nov. 1994, vol. 23, (no.8):597-625.

Swaroop, D. and Hedrick, J.K., "String Stability of Interconnected Dynamic Systems", *IEEE Transactions on Automatic Control*, March 1996.

Swaroop, D., 1995, "String Stability of Interconnected Systems: An Application to Platooning in Automated Highway Systems", *Ph.D. Dissertation*, University of California, Berkeley, 1995.

Swaroop, D. and Rajagopal, K.R., "Intelligent Cruise Control Systems and Traffic Flow Stability," *Transportation Research Part C : Emerging Technologies*, Vol. 7, No. 6, pp. 329-352, 1999.

Swaroop D. Swaroop, R. Huandra, "Design of an ICC system based on a traffic flow specification," *Vehicle System Dynamics Journal*, Vol. 30, no. 5, pp. 319-44, 1998.

Swaroop, D. and Bhattacharya, S.P., "Controller Synthesis for Sign Invariant Impulse Response," *IEEE Transactions on Automatic Control*, Vol. 47, No. 8, pp. 1346-1351, August, 2002.

Swaroop, D., "On the Synthesis of Controllers for Continuous Time LTI Systems that Achieve a Non-Negative Impulse Response," *Automatica*, Feb 2003.

Texas Transportation Institute Report, "2002 Urban Mobility Study," URL: mobility.tamu.edu

Tomizuka, M. and Hedrick, J.K., "Automated Vehicle Control for IVHS Systems", *Proceedings of the IFAC Conference*, Sydney, 1993.

Unsal, C. and Kachroo, P., "Sliding Mode Measurement Feedback Control for Antilock Braking Systems," *IEEE Transactions on Control Systems Technology*, March 1999, Vol. 7, No. 2, pp. 271-281.

Varaiya, Pravin, "Smart Cars on Smart Roads: Problems of Control," *IEEE Transactions on Automatic Control*, v 38 n 2, p 195-207, Feb 1993.

Watanabe, T., Kishimoto, N., Hayafune, K., Yamada, K. and Maede, N., 1997, "Development of an Intelligent Cruise Control System", *Mitsubishi Motors Corporation Report*, Japan.

Woll, J., 1997, "Radar Based Adaptive Cruise Control for Truck Applications", *SAE Paper No. 973184*, Presented at SAE International Truck and Bus Meting and Exposition, Cleveland, Ohio, November 1997.

United States Department of Transportation, *NHTSA, FARS and GES*, "Fatal Accident Reporting System (FARS) and General Estimates System (GES)," 1992.

Yanakiev, D. and Kanellakopoulos, I., 1995, "Variable time Headway for String Stability of Automated Heavy-Duty Vehicles", *Proceedings of the 34th IEEE Conference on Decision and Control*, New Orleans, LA, December 1995, pp. 4077-4081.

Yi, J., Alvarez, L., Claeys, X. and Horowitz, R., "Emergency Braking Control with an Observer Based Dynamic Tire Road Friction Model and Wheel Angular Velocity Measurement," *Vehicle System Dynamics*, 2003, Vol. 39, No. 2, pp. 81-97.

Yu, J.S., "A Robust Adaptive Wheel-Slip Controller for Antilock Brake System," *Proceedings of the 36th IEEE Conference on Decision and Control*, Dec 1997, pp. 2545-2546.